Theory of dynamic nuclear polarization and feedback in quantum dots

Sophia E. Economou[1] and Edwin Barnes[2]
[1]*Naval Research Laboratory, Washington, DC 20375, USA*
[2]*Condensed Matter Theory Center and Joint Quantum Institute, Department of Physics, University of Maryland, College Park, Maryland 20742-4111, USA*
(Received 2 January 2014; revised manuscript received 21 March 2014; published 2 April 2014)

An electron confined in a quantum dot interacts with its local nuclear spin environment through the hyperfine contact interaction. This interaction combined with external control and relaxation or measurement of the electron spin allows for the generation of dynamic nuclear polarization. The quantum nature of the nuclear bath, along with the interplay of coherent external fields and incoherent dynamics in these systems renders a wealth of intriguing phenomena seen in recent experiments such as electron Zeeman frequency focusing, hysteresis, and line dragging. We develop in detail a fully quantum, self-consistent theory that can be applied to such experiments and that moreover has predictive power. Our theory uses the operator sum representation formalism in order to incorporate the incoherent dynamics caused by the additional, Markovian bath, which in self-assembled dots is the vacuum field responsible for electron-hole optical recombination. The beauty of this formalism is that it reduces the complexity of the problem by encoding the joint dynamics of the external coherent and incoherent driving in an effective dynamical map that only acts on the electron spin subspace. This, together with the separation of time scales in the problem, allows for a tractable and analytically solvable formalism. The key role of entanglement between the electron spin and the nuclear spins in the formation of dynamic nuclear polarization naturally follows from our solution. We demonstrate the theory in detail for an optical pulsed experiment and present an in-depth discussion and physical explanation of our results.

DOI: 10.1103/PhysRevB.89.165301 PACS number(s): 76.60.Es, 03.65.Yz, 73.21.La, 78.67.Hc

I. INTRODUCTION

The electron-nuclear spin dynamics in quantum dots (QDs) have attracted intense experimental and theoretical attention in recent years [1–16]. This is both because of the role of the nuclear environment in potential applications in quantum information and because this is an inherently interesting system that exhibits rich physics, especially in the presence of external coherent and incoherent driving.

From a practical point of view, the nuclear spins comprise the main source of electron spin decoherence that limits the quality of spin qubits. On the other hand, the ability to polarize the nuclear spins allows them to be used as an asset instead of a liability. For example, in the singlet-triplet qubit in electrostatically defined QDs, the nuclear polarization is used as an effective magnetic field to implement (psuedo)spin rotations [17]. An ambitious role of the nuclear spins that would take advantage of their long coherence times is their use as a quantum memory, an idea that was proposed [18] but not yet demonstrated experimentally in QDs. Finally, an additional motivation for gaining control over nuclear polarization and controlling the nuclear spins is that a polarized and/or narrowed nuclear bath polarization distribution would have less of a detrimental effect on the electron spin coherence due to a reduction of fluctuations originating from a reduced available phase space to which quantum information can be lost [19,20]. In the case of gate-defined QDs, it was demonstrated that significant amounts of nuclear polarization or distribution narrowing can be generated and stabilized in a controlled fashion [21–23] and that this can give rise to an enhancement of the spin coherence time by nearly an order of magnitude [22]. In the context of self-assembled QDs, a similar effect was achieved via coherent population trapping, with an improvement in coherence time by a factor of several hundred [6].

From a fundamental science point of view, the *open* and *driven* electron-nuclear spin system is of great interest, as it has yielded a number of unexpected and intriguing phenomena [24,25]. These arise from the fact that driving the electron when it is coupled to a reservoir (this can be, for example, a photon or phonon bath or cotunneling with the leads) can produce dynamic nuclear spin polarization (DNP), which in turn feeds back to the electron dynamics. This often causes a reduction in nuclear spin fluctuations, which manifests in a variety of effects depending on the experimental setup. Noteworthy phenomena include synchronizing of the electron spin frequency to that of a periodic train of pulses, which can effectively homogenize an ensemble of spins with a distribution of g factors [4], locking of a driven optical transition to the laser [5,26], and hysteresis in the spectra due to memory effects [5,6,8,26,27]. There exist several theoretical works that analyze DNP processes in various experimental contexts. In the case of gate-defined QDs, a range of phenomena has been studied, such as DNP formation and feedback [28–30], nuclear spin squeezing [31], dark state formation [29,32], entanglement dynamics [31,33], and dynamical self-quenching [34]. In the context of self-assembled QDs, there exist several works that treat the problem of driving with a single continuous laser that showed nuclear feedback effects and hysteresis [35,36], as well as for driving with two phase-locked pulses to achieve tunable polarization [37] and nuclear spin cooling [38].

II. OVERVIEW OF OUR APPROACH

Many of the experimental signatures of DNP repeat across different setups in terms of driving sequences and charge configurations in the QD. It is thus natural to seek

a common theoretical framework which can be adapted to explain any such type of experiment. In addition to the need for understanding existing experimental results, a successful theory should also have predictive power. The difficulty in setting up such a theory for this system is the complexity of the problem: It is an *open* and *driven* system which involves many degrees of freedom, namely the electron spin, excited electronic states outside the electron spin subspace, the nuclear spins, and the reservoir that causes the nonunitary dynamics. Moreover, there are feedback effects: The generated nuclear spin polarization acts as an effective magnetic field on the electron spin. Thus, the state of the latter changes based on this updated magnetic field. The problem clearly has to be solved self-consistently.

In this paper, we lay the foundations of such a theory by expanding on the formalism introduced in our earlier work [39]. Our theory is based on the use of dynamical maps. This is a powerful tool that describes nonunitary evolution through operators that act on the density matrix of the electron spin and evolve it in a nonunitary fashion while preserving its trace. These operators are found by solving for the dynamics of the electron system driven by external fields and interacting with the reservoir. By solving for the effect of these interactions on the electron spin, we can eliminate any additional states outside the qubit subspace and the degrees of freedom of the reservoir, while in principle accounting for their effects *exactly*. This can allow for an analytical approach that offers a general, tractable, and transparent treatment of the problem.

Using the dynamical map that we find for the electron spin evolution under the driving and coupling to the reservoir, we calculate the steady-state electron spin vector, which constitutes our zeroth-order solution (i.e., no coupling to nuclear spins). To include nuclear effects, we perform a perturbative treatment on this zeroth-order solution by finding the response of a single nuclear spin to the motion of the electron spin under the external control. We thus make the independent nuclear spin approximation. By including the hyperfine coupling between the nucleus and electron, we find the joint state of the two spins, which now includes quantum correlations.

In this paper, we focus primarily on a large class of experiments in which the driving is sufficiently fast that the electron spin reaches its dynamical equilibrium steady state quickly compared to both the electron spin decoherence time and the time scale of nuclear spin evolution. The so-called mode-locking experiments [4,40,41] are examples from this class, as is demonstrated in the present work [42]. For these types of experiments, we can employ a Markovian approximation to separate the nuclear spin degrees of freedom from those of the electron, which gives us an effective dynamical map for the nuclear spin. The Markovian approximation is not only valid when the electron dynamics are fast; it is also physically well motivated by noting that when the relaxation to the steady state is fast compared to decoherence, which is in turn fast relative to nuclear dynamics, the electron spin will tend to remain in the steady state it attains in the absence of the nuclear spin. While the electron spin steady state is approximately unaffected by a single nuclear spin, it will change significantly when the full nuclear spin ensemble is taken into account. This is explained in detail in the next paragraph. Working in this Markovian limit, we obtain an expression for the steady state of the nuclear spin which explicitly involves all the parameters of the problem, as well as the electron steady state. To describe continuous wave driving and similar types of experiments, it may be necessary to go beyond the Markovian limit. However, the theory presented in this work can still be adapted to these cases as well, as was done recently to explain experimental data for Ramsey fringes of hole spins; see Ref. [44].

To take into account many-body multinuclear effects, we perform a shift of the Zeeman frequency of the electron by the total effective magnetic field of all nuclear spins (Overhauser shift). This is done by first finding a distribution for the nuclear spin polarization using a mean-field approach. We do this by solving a kinetic equation that determines the probability $P(m)$ that the net nuclear polarization is m. The quantity that enters in this kinetic equation is the single-nucleus flip rate. Note that generally the probability to flip from up to down is different than that to flip from down to up. Both of these rates are found by solving the equation of motion of the single nuclear spin. With the nuclear polarization distribution at hand, we then perform the Overhauser shift and find the average steady-state electron spin vector self-consistently.

To explicitly demonstrate our formalism, in the second part of the paper we focus on the spin mode-locking experiments [4,40] in which a train of fast circularly polarized pulses is applied to the electron. We show that our theory reproduces the main experimental features, including the buildup of nuclear spin polarization and its role in electron spin frequency synchronization [4] and antisynchronization [40] with the pulse train. Furthermore, in this work we go beyond the high magnetic field approximation of Ref. [39] by taking into account the so-called spontaneously generated coherence phenomenon [45], which strongly modifies the generation of electron spin polarization at low magnetic fields [46,47]. We find that in this regime there is larger nuclear spin polarization compared to the higher magnetic field case, but that it takes a longer time to reach the steady state.

We also examine modifications to the mode-locking experimental setup. In particular, we calculate the dynamics when an additional, coherent spin-echo pulse is included in each period. Such pulses are important in the context of quantum information as they constitute the simplest form of dynamical decoupling. We show that this pulse sequence leads to strong electron spin polarization in the plane transverse to the magnetic field, modifies the synchronization effect, and overall reduces the average nuclear spin polarization.

This paper is organized as follows. In Sec. III we give an intuitive explanation of DNP in terms of electron-nuclear spin entanglement. In Sec. IV we present a brief review of the operator sum formalism, and in Sec. V we motivate and review our general formalism. Section VI is devoted to analyzing and explaining the pulsed mode-locking experiments [4,40].

III. DYNAMIC NUCLEAR POLARIZATION IN QUANTUM DOTS

Dynamic nuclear polarization is nuclear polarization generated through dynamic processes, most commonly external driving fields and some kind of incoherent dynamics of the electron spin, instead of by simple nuclear spin relaxation

(cooling) to a polarized ground state. Overhauser was the first to predict such an effect in the early 1950s [48], and his prediction was originally met with skepticism until it was verified by Slichter and Carver [49]. Since then, there has been a huge number of DNP experiments conducted in a variety of diverse systems and based on various nonunitary physical processes. A key component of DNP is clearly a mechanism that removes entropy from the system. Such nonunitary mechanisms may correspond to relaxation or measurement. In the case of self-assembled QDs the experiments are optical and involve an excited state outside the electron spin subspace, typically a charged exciton, created by a (quasi) resonant laser focused on the band gap. The extraction of entropy from the system happens through optical excitation followed by recombination and spontaneous emission of a photon. The emitted photon generally carries information about the system and can therefore lower the entropy of the net electron-nuclear state. Experimentally, this can coincide with the actual measurement of the system, but this is not necessarily always the case.

Optical experiments in QDs have revealed a distinct incarnation of the DNP effect and rich physics based on the interplay of the optical driving, the spontaneous recombination, and of course the quantum many-body nuclear bath. It is perhaps useful at this point to discuss what distinguishes these DNP experiments with QDs from more conventional DNP demonstrations. One feature of the QD is that it involves a large number of nuclear spins, about 10^4–10^6, depending on dot size. Therefore, the nuclear spectra can be thought of as bands instead of discrete energy levels and generally cannot be resolved by the external fields.

A more important feature, however, is the role of nuclear feedback. As mentioned above, nuclear polarization acts as an effective magnetic field that shifts the Zeeman frequency of the electron spin. The distinctive feature in QD experiments is that there exist selection rules which affect electron spins differently depending on their orientation and energy. Therefore, a shift in the Zeeman splitting is not just a small quantitative correction, but can instead change *qualitatively* the behavior of the system. For example, in the optical mode-locking experiment an electron with a Larmor period that is an integer multiple of the pulse repetition period will become fully polarized and will subsequently be insensitive to the pulse due to polarization selection rules. On the other hand, an electron with a Larmor period that is a half-integer multiple of the period will be minimally polarized by the pulse train. This example demonstrates how the nuclear feedback can have a large effect on the behavior of the electron spin and why a self-consistent treatment is necessary.

To close this section let us present the physical picture of DNP generation in QDs via a toy model [50]. Consider two spins, one initialized in a pure state and the other in a mixed state, corresponding to the electron and nuclear spin, respectively. Now allow them to evolve under a Heisenberg type interaction $A\mathbf{S}_1 \cdot \mathbf{S}_2$. The evolution from the initial state to the state at time $t = \pi/A$ is described as

$$|\uparrow\rangle\langle\uparrow|\otimes(|\uparrow\rangle\langle\uparrow|+|\downarrow\rangle\langle\downarrow|) \rightarrow (|\uparrow\rangle\langle\uparrow|+|\downarrow\rangle\langle\downarrow|)\otimes|\uparrow\rangle\langle\uparrow|.$$

In the language of quantum information, we can view this as a SWAP gate, meaning that the two spins have swapped quantum states. Now at $t = \pi/A$ a pulse comes in which performs a projective measurement on the first spin and collapses it, e.g., into state $|\downarrow\rangle$. This process leaves *both* spins in a pure (i.e., fully polarized) state even though the nuclear spin never interacted directly with the external field. This is precisely the process that removes entropy from the system via the measurement. The purpose of this toy model is to demonstrate this effect in a straightforward manner and hopefully build intuition into the more complicated dynamics that we present below.

IV. OPERATOR SUM REPRESENTATION (KRAUS) FORMALISM

In quantum mechanics, a closed system undergoes unitary evolution. However, that is not the most general type of evolution. A system generally interacts with other systems, and energy and entropy can be exchanged with them through this interaction. The system is then called open, and the operator sum representation formalism can be used to describe its nonunitary evolution. The operators that describe this irreversible evolution are called Kraus operators [52], and they act on a density matrix ρ in the following way:

$$\rho' = \sum_k E_k \rho E_k^\dagger, \tag{1}$$

where $k > 1$ and the relation

$$\sum_k E_k^\dagger E_k = \mathbb{1}$$

(where $\mathbb{1}$ is the identity operator) should hold in order to guarantee that the trace of the density matrix remains equal to one. As a simple example, consider a two-level system where the population can relax from the excited to the ground state irreversibly. This is an ubiquitous scenario across physical systems; e.g., this may be an atom in a metastable optically excited state, or a nuclear spin, etc. The Kraus operators that describe the decay from the excited to the ground state are (in the basis $\{|g\rangle,|e\rangle\}$)

$$M_0 = \begin{bmatrix} 1 & 0 \\ 0 & \sqrt{\alpha} \end{bmatrix}, \quad M_1 = \begin{bmatrix} 0 & \sqrt{1-\alpha} \\ 0 & 0 \end{bmatrix}. \tag{2}$$

Starting from an arbitrary initial density matrix,

$$\rho = \begin{bmatrix} \rho_{11} & \rho_{12} \\ \rho_{21} & \rho_{22} \end{bmatrix}, \tag{3}$$

the final density matrix after the probabilistic decay process has completed is then

$$\rho' = \begin{bmatrix} \rho_{11} + (1-\alpha)\rho_{22} & \sqrt{\alpha}\rho_{12} \\ \sqrt{\alpha}\rho_{21} & \alpha\rho_{22} \end{bmatrix}. \tag{4}$$

It is simple to check that when $\alpha = 0$ we have complete relaxation from the excited to the ground state, while $\alpha = 1$ yields the trivial solution of no decay, with the system remaining in its initial state without evolving. It is useful to note here that one could make α a time-dependent parameter. In that case, the density matrix can be found at any time using Eq. (1). For exponential decay, we would have $\alpha = \alpha(t) = e^{-t/T_1}$, while the decoherence, described by the decay of the

off-diagonal density matrix component, occurs with a time scale $T_2 = 2T_1$, as it should.

V. GENERAL FORMALISM

The total Hamiltonian of the system is

$$H(t) = H_{0,e} + H_c(t) + H_{\rm res} + H_{0,n} + H_{hf}, \tag{5}$$

where $H_{0,e}$ is the free part of the electron Hamiltonian in the QD, $H_c(t)$ is the control Hamiltonian, and $H_{\rm res}$ is the interaction with the reservoir. We focus on the case where $H_c(t) = H_c(t + T_R)$ describes a periodic sequence of finite-duration pulses with a period T_R. In general, these pulses will couple the electron spin states to higher excited levels. All the population decays back to the electron spin subspace through the interaction with the reservoir, $H_{\rm res}$, with characteristic rate γ. In self-assembled dots, $H_c(t)$ describes optical pulses coupling the electron spin states to additional levels that are charged excitons, also called trions, and $H_{\rm res}$ is the photon bath. In electrostatically defined QDs, $H_c(t)$ is a gate voltage, the additional states can be, for example, the two polarized triplet states that lie outside the singlet-triplet qubit subspace, and $H_{\rm res}$ represents the interaction with the leads. The remaining two terms are the nuclear spin Hamiltonian in the presence of a magnetic field, $H_{0,n} = \omega_n \sum_i \hat{I}^i_z$, and the hyperfine interaction between the electron and N nuclei,

$$H_{hf} = \sum_{i=1}^{N} A_i \hat{S}_z \hat{I}^i_z + \sum_{i=1}^{N} A_i/2(\hat{S}_+ \hat{I}^i_- + \hat{S}_- \hat{I}^i_+). \tag{6}$$

The first term in H_{hf} is referred to as the Overhauser term, while the second is known as the flip-flop term. The hyperfine couplings are determined by the magnitude of the electronic wave function at the locations of the nuclear spins: $A_i = \mathcal{A} v_0 |\Psi(r_i)|^2$, where $\mathcal{A}$ is the total hyperfine energy, v_0 is the volume per nucleus, Ψ is the electronic wave function, and r_i is the location of the ith nucleus.

There are two features of the open electron-nuclear spin system that are advantageous toward the development of a formalism to treat this problem. The first feature is that the control Hamiltonian, $H_c(t)$, acts solely on the electron spin subsystem and does not directly affect the nuclear spins. This fact, combined with the smallness of the hyperfine couplings compared with the electron Zeeman frequency, allows us to first solve for the electron evolution in the absence of the nuclei and to then compute the response of the nuclear spins to the electron dynamics. Specifically, we employ a perturbative expansion in the hyperfine flip-flop interaction to obtain analytical expressions for the nuclear steady state and relaxation rate.

The second useful feature is a hierarchy of time scales. In particular, we primarily focus on experiments in which the reservoir-induced relaxation from auxiliary excited states to the electron spin subspace is fast compared to the driving period: $\gamma T_R \gg 1$. This allows us to describe the evolution over one period in terms of a dynamical map that acts only on the 2×2 electron spin subspace instead of a larger dimensional Hilbert space. This in turn enables us to coarse-grain the electron spin evolution by piecing together copies of this dynamical map, leading to a substantial simplification of the analysis, and allowing for greater insight into the physics. We also take advantage of a second time scale hierarchy, namely $\tau_e \ll T_2 \ll \tau_n$, where τ_e is the time it takes for the electron to reach its steady state, T_2 is the decoherence time of the electron spin, and τ_n is a characteristic time scale for nuclear dynamics. In this regime, decoherence works to keep the electron spin in the steady state it would have in the absence of nuclei, although the nuclear Overhauser field will still induce a shift in the electron Zeeman frequency. This indicates that a Markovian approximation in which electron-nuclear correlations are discarded after each driving period is not only justified but physically well motivated. Note that, even in systems where these time-scale hierarchies do not hold (such as in singlet-triplet qubits), so long as there is a nonunitary process that resets the qubit, we would still expect a Markovian approximation to apply. One difference, however, is that instead of first calculating the electron spin steady state alone, one may need to calculate the total electron-nuclear spin (nonunitary) evolution per cycle.

In the following sections, we describe in detail our general formalism as it applies to the large class of experiments exhibiting the time scale hierarchies described above. The first step is to derive the dynamical map describing the evolution of the electron system without the hyperfine interactions and to use this result to compute the electron spin steady state. We then couple a single nuclear spin to the electron and calculate its resulting steady state and relaxation rate. These quantities are the ingredients needed to construct the multinuclear flip rates that enter into a kinetic equation for the nuclear spin polarization distribution of the entire nuclear spin ensemble. The solution of this kinetic equation then gives the polarization distribution generated by a particular driving sequence. Finally, we obtain the nuclear feedback on the electron spin steady state by performing an Overhauser shift in the Zeeman frequency and averaging the resulting modified steady state over the polarization distribution. In the second half of the paper, we apply our formalism to the particular case of the mode-locking experiments [4,40]. We demonstrate explicitly the requisite hierarchy of time scales, and we show that our formalism reproduces the salient features of the experimental findings.

A. Electron spin Kraus operators

To find the zeroth-order solution as a 2×2 operation on the electron spin only, we first take the standard approach of treating the reservoir to second order under the Markovian approximation, which gives rise to decay and decoherence terms in the Liouville-von Neumann equation. These terms can be described by Lindblad operators so that, ignoring nuclear terms and defining $H_e(t) = H_{0,e} + H_c(t)$, the total evolution for the electron subsystem is described by

$$\dot{R} = i[R, H_e(t)] + \mathcal{L}(R), \tag{7}$$

where the symbol R is used to stress that this density matrix includes the two spin states *and* the excited states that couple to the spin subspace via $H_c(t)$. It is important to note that the initial condition for (7) is an arbitrary density matrix *in the spin subspace*, i.e., only a 2×2 block of nonzero matrix elements. Since we are interested only in the spin subspace, we would

like to use Eq. (7) to construct a dynamical map that describes only the evolution of this subspace in terms of 2×2 matrices. To facilitate this construction, we focus on the regime in which the relaxation is fast compared to the pulse period ($\gamma T_R \gg 1$). Since the theory can be applied for multiple pulses per period, a more precise condition would, in fact, be that $1/\gamma$ should be small compared to the largest time delay between pulses that occurs in the pulse sequence. In this case, the density matrix R after one period is such that the components outside the 2×2 spin subspace block are negligibly small, and we can derive a dynamical map that evolves the spin subspace over one period T_R. For one or even two excited states, this can often be done analytically. Otherwise, a perturbative or numerical approach is needed. The solution either way will provide an expression for ρ', the density matrix of the electron spin after one period, as a function of the initial density matrix ρ. From this we can extract the Kraus operators $\{\mathcal{E}_k\}$ since they are used to relate ρ' to ρ:

$$\rho' = \sum_k \mathcal{E}_k \rho \mathcal{E}_k^\dagger. \tag{8}$$

Note that the $\{\mathcal{E}_k\}$ contain the evolution of the whole period, including both the unitary part due to the free Hamiltonian and the coherent control effects and the nonunitary part due to the reservoir. The explicit form of the Kraus operators for pulsed experiments are given in Sec. VI.

B. Spin-vector representation

For the present problem, the density matrix is not a convenient representation of the spin state. The reason is that to find the steady state of the electron spin, we need to operate on it with the appropriate Kraus operators an infinite number of times, and since these operators act on both sides of the density matrix, this quickly becomes intractable. A much more convenient way to solve this problem is to transform to the spin-vector (SV) representation, which is a completely equivalent way of representing the state of the system, but with the important property that the operators describing the evolution act on the left only [52]. In addition, the SV representation offers a compelling geometric visualization of the dynamics.

Before we proceed with the derivation of the SV representation from Eq. (8), let us first discuss what kind of physics the dynamical map of the spin should describe. Obviously, the evolution will generally be nonunitary, but what does that mean for an input state? Clearly, a pure state undergoing nonunitary evolution will generally *lose* purity and will become (partially or fully) mixed. Note, however, that a mixed state may either become *more* or *less* mixed under nonunitary evolution. The latter case, where the system gains purity, is equivalent to increasing the spin polarization in the system. In the special case of zero initial polarization, the pulse and subsequent reservoir-induced relaxation will generate a nonzero SV after one driving period. We thus expect the general form of the evolution of the SV S over one period to be given by

$$S' = YS + K, \tag{9}$$

where S and S' correspond to density matrices ρ and ρ', respectively, in Eq. (8). We define the SV to be normalized to unity; i.e., its components are given by $S_m = \mathrm{Tr}(\rho\sigma_m)$, where σ_m denotes the Pauli matrices. In general, the matrix Y both rotates and shrinks the SV due to population loss, while K restores the population to the electron spin Hilbert space. To find Y and K we start from the general equation

$$\rho' = \sum_j \mathcal{E}_j \rho \mathcal{E}_j^\dagger \tag{10}$$

and multiply both sides by the Pauli matrix σ_ℓ and take the trace:

$$\mathrm{Tr}(\sigma_\ell \rho') = \mathrm{Tr}\left(\sum_j \sigma_\ell \mathcal{E}_j \rho \mathcal{E}_j^\dagger\right). \tag{11}$$

The left-hand side is just S_ℓ, and we express ρ on the right-hand side in terms of the SV; i.e., we make the substitution $\rho = 1/2 + 1/2 \sum_m \sigma_m S_m$ to obtain

$$S'_\ell = K_\ell + \sum_m Y_{\ell,m} S_m, \tag{12}$$

where

$$K_\ell = \frac{1}{2}\mathrm{Tr}\sum_j \sigma_\ell \mathcal{E}_j \mathcal{E}_j^\dagger = \mathrm{Tr}\sum_j s_\ell \mathcal{E}_j \mathcal{E}_j^\dagger, \tag{13}$$

$$Y_{\ell,m} = \frac{1}{2}\mathrm{Tr}\sum_j \sigma_\ell \mathcal{E}_j \sigma_m \mathcal{E}_j^\dagger = 2\mathrm{Tr}\sum_j s_\ell \mathcal{E}_j s_m \mathcal{E}_j^\dagger, \tag{14}$$

where we define $s_j = \frac{1}{2}\sigma_j$.

C. Zeroth-order solution: The steady-state electron spin vector

An unpolarized spin undergoing the evolution described by Y and K will obtain some polarization. The spin right after the first, second, and nth driving period will be, respectively,

$$\begin{aligned} &S_1 = K, \quad S_2 = YS_1 + K = YK + K, \\ &S_n = YS_{n-1} + K = (Y^{n-1} + \cdots + Y + \mathbb{1})K. \end{aligned} \tag{15}$$

Equation (15) is a geometric series; we can therefore readily write down the expression for the steady-state SV *at the end* of a driving period as

$$S_\infty = (\mathbb{1} - Y)^{-1} K. \tag{16}$$

The inverse in the above equation in general exists because the eigenvalues of Y are all less than unity, as follows from the fact that Y includes the loss of population to the excited state. Before we proceed to the inclusion of the nuclear spin, we consider a slightly modified, but equivalent, version of this formalism, where the vector K and the matrix Y are represented by a single 4×4 matrix:

$$\mathcal{Y}_e = \begin{bmatrix} 1 & 0 & 0 & 0 \\ K_x & Y_{xx} & Y_{xy} & Y_{xz} \\ K_y & Y_{yx} & Y_{yy} & Y_{yz} \\ K_z & Y_{zx} & Y_{zy} & Y_{zz} \end{bmatrix}. \tag{17}$$

It is easy to check that in this four-dimensional (4D) representation, the steady-state SV $\mathcal{S}_e^{(\infty)} = (1, S_{e,x}^{(\infty)}, S_{e,y}^{(\infty)}, S_{e,z}^{(\infty)})$ is the eigenvector of $\mathbb{1} - \mathcal{Y}_e$ with eigenvalue zero. It is generally the

case that the first component of the 4D SV must remain fixed at 1 in order for $\mathcal{Y}_e$ to evolve the remaining three components of the SV appropriately. This more compact representation will prove very useful when we introduce the nuclear spin.

D. Including a single nuclear spin

The next goal is to find an equation similar to Eq. (9) for the nuclear spin and from that derive the steady-state nuclear SV along with the relaxation rate. These quantities will later be used as inputs into the equation that determines the nuclear polarization distribution for the entire ensemble of N nuclear spins. For simplicity, we focus on the case of spin-$\frac{1}{2}$ nuclei throughout the paper, but the formalism could be extended to consider other species of nuclei as well.

We begin by finding the appropriate Kraus operators for the two-spin system. Here we are keeping them arbitrary since we are interested in presenting the general method, but in Sec. VI we derive the Kraus explicitly for the pulsed problem. Defining the two-spin Kraus operators as $\mathcal{F}_j$, we evolve the density matrix $\mathcal{P}$ describing the total electron-nuclear spin state over one driving period according to

$$\mathcal{P}' = \sum_j \mathcal{F}_j \mathcal{P} \mathcal{F}_j^\dagger. \tag{18}$$

Let us now define generalized Pauli matrices for the two-spin system, which are tensor products of the usual Pauli matrices, including unity,

$$G_{4k+\ell} = s_k \otimes s_\ell, \tag{19}$$

where k,ℓ run from 0 to 3, with $s_0 \equiv \frac{1}{2}\mathbb{1}$. Using these operators, we can define the SV for the joint system. There are 16 different G's, but only 15 numbers are needed to specify the state due to the normalization constraint. However, in analogy to the 4D SV representation defined above, we work in a 16D representation in which $\mathcal{S}$ denotes the two-spin SV containing both the electronic and nuclear spin degrees of freedom, i.e., $\mathcal{S}_i = 4\mathrm{Tr}(\mathcal{P}G_i)$. In general, $\mathcal{S}$ is not simply a tensor product of the two individual SVs, but contains quantum correlations between the electron and nuclear spins. In this representation, the evolution operator over one period is given by

$$\mathcal{Y}_{ij} = 4\sum_\ell \mathrm{Tr}[G_i \mathcal{F}_\ell G_j \mathcal{F}_\ell^\dagger], \tag{20}$$

with the total SV evolving according to

$$\mathcal{S}' = \mathcal{Y}\mathcal{S}. \tag{21}$$

In principle, we could obtain the two-spin steady state by finding the eigenvector of $\mathbb{1} - \mathcal{Y}$ with vanishing eigenvalue in direct analogy with the single electron spin case treated above. However, we instead perform a Markovian approximation which amounts to keeping only the separable (tensor product) part of $\mathcal{S}$, i.e., $\mathcal{S} \approx \mathcal{S}_e^{(\infty)} \otimes \mathcal{S}_n$. As discussed above, this approximation is valid when there is a separation of time scales, in particular when the electron reaches its steady state, $\mathcal{S}_e^{(\infty)}$, quickly compared to the nuclear dynamics and the electron spin decoherence time. When this is the case, the electron tends to remain in the steady state it would have without interactions with the nuclei, suggesting that the Markovian treatment is, in fact, more physical. We then obtain the effective nuclear spin evolution $\mathcal{Y}_n$ by acting with $\mathcal{Y}$ on the tensor product $\mathcal{S}_e^{(\infty)} \otimes \mathcal{S}_n$ and reading off the coefficients of the components of $\mathcal{S}_n$ from the resulting $\mathcal{S}'$. This procedure can be summarized by the equation

$$(\mathcal{Y}_n)_{\alpha\beta} = \frac{d}{d\mathcal{S}_{n,\beta}}\left[\mathcal{Y}\left(\mathcal{S}_e^{(\infty)} \otimes \mathcal{S}_n\right)\right]_\alpha, \tag{22}$$

where the resulting $\mathcal{Y}_n$ explicitly contains electron SV components. From $\mathcal{Y}_n$ we find the nuclear spin steady state $\mathcal{S}_n^{(\infty)} = (1, S_{n,x}^{(\infty)}, S_{n,y}^{(\infty)}, S_{n,z}^{(\infty)})$ as the eigenvector of $\mathbb{1} - \mathcal{Y}_n$ with eigenvalue equal to zero.

Next, we explain how to derive the nuclear relaxation rate. The evolution of the 4D nuclear SV is described by

$$\mathcal{S}_n(t + T_R) = \mathcal{Y}_n \mathcal{S}_n(t). \tag{23}$$

Since the nuclear evolution is much slower than T_R, we can coarse grain this equation to obtain a differential equation for the nuclear SV,

$$\frac{d}{dt}\mathcal{S}_n = \frac{1}{T_R}(\mathcal{Y}_n - \mathbb{1})\mathcal{S}_n, \tag{24}$$

which gives

$$\mathcal{S}_n(t) = e^{(\mathcal{Y}_n - \mathbb{1})t/T_R}\mathcal{S}_n(0). \tag{25}$$

It is clear from this result that the smallest nonzero eigenvalue, λ_2, of $\mathbb{1} - \mathcal{Y}_n$ will determine the relaxation rate of the nuclear spin: $\gamma_n = \lambda_2/T_R$.

E. Nuclear spin steady state and relaxation rate in the perturbative regime

In the previous section, we showed that in the Markovian limit, the nuclear steady state and relaxation rate can be obtained from the effective evolution operator (in the SV representation) for a single nuclear spin over one period, $\mathcal{Y}_n$. Specifically, the steady state is given by the eigenvector of $\mathbb{1} - \mathcal{Y}_n$ with eigenvalue zero, while the relaxation rate is inversely proportional to the smallest nonzero eigenvalue of $\mathbb{1} - \mathcal{Y}_n$. In order to obtain explicit analytical results, we make use of the fact that the hyperfine couplings are small compared to the electron Zeeman energy and perform a perturbative expansion in the hyperfine flip-flop interaction. We keep the Overhauser part of the interaction to all orders in the coupling [see Eq. (6)]. In Appendix A, we show that to leading order in this perturbative expansion, the nuclear spin steady state has the form

$$\mathcal{S}_n^{(0)} = (1,0,0,\xi^*), \tag{26}$$

where the nuclear spin components transverse to the magnetic field vanish to leading order. It is further shown in the appendix how to explicitly calculate ξ^* as well as the smallest nonzero eigenvalue, λ_2^*, of $\mathbb{1} - \mathcal{Y}_n$. These quantities are used below to determine the nuclear spin-flip rates.

F. Driving with a simple periodic pulse train

An important class of driving sequences involves a periodic pulse train with a single pulse per period. This includes, but is not limited to, the case of mode locking, which is analyzed in depth below. For this class of driving sequences, the explicit expressions for each term in the perturbative

hyperfine expansion of $\mathcal{Y}_n$ up to second order are given in Appendix B, and the full expressions for $\xi^* = S_{n,z}^{(\infty)}$ and λ_2^* are given in Appendix C. In the remainder of the paper, we denote the nuclear spin steady state by $S_n^{(\infty)}$. In the limit $\omega_n \to 0$, the expressions for $S_{n,z}^{(\infty)}$ and λ_2^* reduce to the results quoted in Ref. [39]:

$$S_{n,z}^{(\infty)} = \frac{S_{e,z}\left[\left(S_e^2-1\right)\cos\left(\frac{AT_R}{2}\right)+S_e^2+1\right]}{S_{e,z}^2+\left(S_e^2-1\right)\cos\left(\frac{AT_R}{2}\right)+1}, \tag{27}$$

$$\lambda_2^* = \frac{A^2}{\omega_e^2}\frac{1+S_{e,z}^2+\left(S_e^2-1\right)\cos\left(\frac{AT_R}{2}\right)}{1+S_{e,z}^2+\left(S_{e,z}^2-1\right)\cos\left(\frac{AT_R}{2}\right)}\sin^2\frac{\omega_e T_R}{2}. \tag{28}$$

In the above expressions, we have compressed the notation for the electron steady state $S_{e,i}^{(\infty)} \to S_{e,i}$ for the sake of brevity, and we have defined $S_e^2 \equiv S_{e,x}^2 + S_{e,y}^2 + S_{e,z}^2$.

Given the generality of Eqs. (27) and (28) it is worth pausing for a moment to examine the physical content of these expressions. First, the fact that $S_{n,z}^{(\infty)}$ is proportional to $S_{e,z}^{(\infty)}$ is a reflection of conservation of angular momentum, which requires that $S_{n,z}^{(\infty)} = 0$ when $S_{e,z}^{(\infty)} = 0$. Second, it can be seen from Eq. (28) that when $AT_R \ll 1$ (as is typically necessary for the validity of the Markovian approximation) and when the electron spin is polarized primarily along the directions transverse to the magnetic field (e.g., $S_{e,x}^{(\infty)} \approx 1$), λ_2^* and hence γ_n become very large, leading to rapid flipping of the nuclear spin. This behavior can be attributed to the fact that the electron spin flips more easily when it is polarized transversely to the B field since in this case hyperfine flip-flops do not violate energy conservation. On the other hand, when the electron spin is polarized along the magnetic field direction, flip-flops are suppressed due to the large Zeeman energy mismatch between the electron and nuclear spins.

Third, we point out the factor $\sin^2\frac{\omega_e T_R}{2}$ in Eq. (28), which indicates the importance of the driving period relative to the Zeeman frequency. In particular, we would like to address why the rate is zero when the electron spin has a precession period that is commensurate with the driving period, while it is maximized when the precession period is a half-integer multiple of the driving period. To understand this, we consider a simple model in which the driving is a train of pulses, each acting on one of the two electron spin states along the magnetic field, i.e., the eigenstates of the free electron Hamiltonian, and exciting that state to an auxiliary, trion level. For concreteness we choose to drive the spin-down state, $|\downarrow\rangle$. We consider the simplest case of an instantaneous, resonant pulse, such that the electron spin steady state in the absence of nuclei is simply the other spin state, $|\uparrow\rangle$, i.e., $S_{e,z} = S_e = 1$. Plugging these values into Eq. (28) we obtain the simple expression $\lambda_2^* = \frac{A^2}{\omega_e^2}\sin^2\frac{\omega_e T_R}{2}$. Now we consider adding a nuclear spin in order to see physically the origin of this expression. In particular, under the Heisenberg-type interaction, the evolution operator of the two-spin system (electron and nuclear spin) after one period is $U_{hf}(T_R) = e^{-i(H_{0,e}+H_{hf})T_R}$.

We consider the two limiting cases mentioned above, $T_R = 2n\pi/\omega_e$ and $T_R = (2n+1)\pi/\omega_e$. Expanding the corresponding evolution operators to second order in A/ω_e, and applying them to a state with $S_{e,z} = S_e = 1$ and an arbitrary nuclear spin state, i.e., $|\uparrow\rangle(c_\uparrow|\uparrow\rangle + c_\downarrow|\downarrow\rangle)$ we obtain the following. When $T_R = \frac{2n\pi}{\omega_e}$,

$$|\uparrow\rangle(c_\uparrow e^{-i\pi\frac{A}{\omega_e}}|\uparrow\rangle + c_\downarrow e^{i\pi\frac{A}{\omega_e}}|\downarrow\rangle), \tag{29}$$

and when $T_R = \frac{(2n+1)\pi}{\omega_e}$,

$$c_\uparrow e^{-i\pi\frac{A}{2\omega_e}}|\uparrow\rangle|\uparrow\rangle + c_\downarrow e^{i\pi\frac{A}{2\omega_e}}|\uparrow\rangle|\downarrow\rangle + \frac{A}{\omega_e}c_\downarrow e^{i\pi\frac{A}{2\omega_e}}|\downarrow\rangle|\uparrow\rangle. \tag{30}$$

Comparing Eqs. (29) and (30) we see that the first is a separable state of the electron and the nuclear spin, while the second contains entanglement. This showcases the importance of entanglement in DNP, as discussed in Sec. III, and how it manifests itself in the actual calculated nuclear relaxation rate. Therefore, we can directly link the sine factor in Eq. (28) to electron-nuclear entanglement and its crucial role in the nuclear spin dynamics.

G. Nuclear polarization distribution

Once we have found the nuclear spin relaxation rate and steady state, the nuclear spin-flip rates are given by (see Appendix D for derivation and assumptions)

$$\mathrm{w}_\pm = \gamma_n\left(1 \pm S_{n,z}^{(\infty)}\right)/2, \tag{31}$$

where w_+ (w_-) is the rate to flip from down (up) to up (down). More precisely, for a single nucleus we may write

$$\frac{dP_\uparrow}{dt} = -\mathrm{w}_- P_\uparrow + \mathrm{w}_+ P_\downarrow, \tag{32}$$

where $P_\uparrow$ is the probability that the nucleus is aligned with the magnetic field and $P_\downarrow = 1 - P_\uparrow$ is the probability that it lies antiparallel to the magnetic field. The flip rates will generally be different, and they will be functions of the various parameters in the problem, including the electron Zeeman frequency ω_e.

Defining the difference in the number of spins pointing up and down as m, the kinetic equation for the distribution of the net multinuclear polarization $m/2$ is

$$\frac{dP(m)}{dt} = -\sum_\pm\left[w_\pm(m)\frac{N\mp m}{2}\right]P(m) + \sum_\pm P(m\pm 2)w_\mp(m\pm 2)\left[\frac{N\pm m}{2}+1\right], \tag{33}$$

where $w_\pm(m)$ are the rates in the presence of nuclear polarization $m/2$. These are found by implementing the Overhauser shift, i.e., taking

$$w_\pm(m) = \mathrm{w}_\pm(\omega_e \to \omega_e + mA/2). \tag{34}$$

In Eq. (34) we have made the so-called "box model" approximation, which amounts to taking all the hyperfine couplings to be equal. This approximation is valid when the electron spin dynamics are rapid relative to the hyperfine scale $N/\mathcal{A}$ [39,53]. This condition is automatically satisfied whenever the driving is fast compared to the electron spin decoherence, which is the experimental regime we are considering. Note that although we are setting all the hyperfine couplings equal, we are not imposing the angular momentum symmetries associated with the box model, which would restrict the nuclear state to

its original total angular momentum subspace, limiting the amount of nuclear polarization that can be generated. Here no such limitation is present, and thus larger nuclear polarization can be generated.

The steady state corresponds to having $dP(m)/dt = 0$, which gives an equation connecting $P(m)$ with $P(m \pm 2)$. Rearranging terms, we can see that

$$\frac{N-m}{2} w_+(m)P(m) - \left[\frac{N+m}{2}+1\right] w_-(m+2)P(m+2) = \left[\frac{N-m}{2}+1\right] w_+(m-2)P(m-2) - \frac{N+m}{2} w_-(m)P(m)$$

holds, which implies that the expression

$$\frac{N-m}{2} w_+(m)P(m) - \frac{N+m+2}{2} w_-(m+2)P(m+2)$$

is a constant. Since the full relation above is invariant with respect to rescalings of $P(m)$, we conclude that this constant is zero. We then have

$$P(m) = \frac{N-m+2}{N+m} \frac{w_+(m-2)}{w_-(m)} P(m-2), \tag{35}$$

which can be solved iteratively by setting the first nonzero entry, $P(-N)$ to some arbitrary value and normalizing the final result: $\sum_m P(m) = 1$.

H. Feedback on electron spin

Having obtained the nuclear polarization distribution for the net multinuclear spin system, we can calculate the updated electron SV by performing the Overhauser shift, i.e., shifting the Zeeman frequency by $mA/2$ and averaging over m:

$$\overline{S}_{e,i} = \sum_{m=-N}^{N} dm\, P(m) S_{e,i}(\omega_e + mA/2). \tag{36}$$

In Eq. (36) it is understood that $\overline{S}_{e,i} \equiv \overline{S_{e,i}^{(\infty)}}$. The quantity that is usually measured experimentally in self-assembled QDs is the component of $\overline{S}_e$ that is parallel (or antiparallel) to the pulse propagation direction. Below we derive an explicit form for this quantity for the pulsed mode-locking experiment.

VI. APPLICATION TO MODE-LOCKING EXPERIMENT

In this section we apply the formalism developed above to the case where there is one fast circularly polarized pulse per period, as depicted in Fig. 1. There is a magnetic field pointing in the plane of the QD, perpendicular to the pulse propagation direction (the so-called Voigt geometry). This is the experiment by Greilich *et al.* [4], where the periodic pumping of an ensemble of singly charged electron dots was shown to modify the nuclear spin environment in these dots, an effect manifested

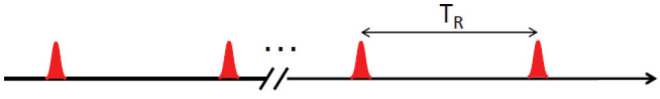

FIG. 1. (Color online) Pulse sequence for the mode-locking experiment.

in the measurement of the electron spin. In particular, there was a nuclear-induced "push" of the electron Zeeman frequency towards those frequencies that were commensurate with the pulse train period. As a result, the ensemble obtained higher electron spin polarization than what one would expect in the absence of the nuclear feedback. In this experiment, resonant pulses of approximately π area were used, meaning that the population transfer from the electron spin state to the optically excited trion state by the pulse was maximal. It was later shown by Carter and collaborators [40] that when detuned pulses are used instead, richer physics emerges as a result of the interplay between coherent and incoherent pulse-induced dynamics. In particular, the detuning causes a nonzero steady-state electron spin component along the magnetic field axis, which in turn renders the nuclear flip rates *directional*, an effect absent in the resonant case of Ref. [4]. Here we treat the general case, where there is a nonzero detuning. We follow the steps analyzed in the sections above for this particular example.

A. Electron spin Kraus operators

The first step is to find the Kraus operators describing the electron spin evolution due to a single pulse and the subsequent spontaneous emission. The Hamiltonian for an electron in a magnetic field along the z axis, in the absence of nuclear spin interactions and in the presence of a train of left-circularly polarized pulses is

$$H_e = \omega_e \hat{S}_z + \epsilon_{\bar{T}} |\bar{T}\rangle\langle\bar{T}| + \sum_k \Omega(t - kT_R)|\bar{x}\rangle\langle\bar{T}| + \text{H.c.} \tag{37}$$

Since the g factor of the hole along the z axis is negligible, the trion state with the opposite spin is ignored. Note that as a result of polarization selection rules, the pulse *only* couples state $|\bar{x}\rangle$, the state with the electron spin pointing antiparallel to the pulse propagation direction, to the trion state $|\bar{T}\rangle$ with angular momentum projection $-3/2$ along the x axis. In the rotating wave approximation, the coupling to the pulse is $\Omega(t - t_o) = \Omega_o f(t - t_o) e^{i\omega(t-t_o)}$. The radiation field will be included in the form of Lindblad operators. We take the pulses to be the fastest time scale in the system, i.e., much faster than the Zeeman precession period and the spontaneous emission time scale. This allows us to treat the pulse as acting instantaneously on the two-level system (composed of $|\bar{x}\rangle$ and $|\bar{T}\rangle$) only. This is a good approximation for these types of ultrafast experiments, where picosecond, or even subpicosecond, pulses are used. Then we find the Kraus operators in two steps. First we consider the coherent effects, i.e., the excitation (and possibly stimulated emission) by the pulse, and treat the resulting state in the three-level Hilbert space as the input to the remaining terms describing spontaneous emission in the presence of the external magnetic field. Defining the evolution operator due to the pulse in the $|x\rangle, |\bar{x}\rangle, |\bar{T}\rangle$ basis as

$$U_p = \begin{bmatrix} 1 & 0 & 0 \\ 0 & u_{\bar{x}\bar{x}} & -u^*_{\bar{T}\bar{x}} \\ 0 & u_{\bar{T}\bar{x}} & u^*_{\bar{x}\bar{x}} \end{bmatrix}, \tag{38}$$

the density matrix of the three-level system right after the pulse is

$$R = U_p R_0 U_p^\dagger = \begin{bmatrix} \rho_{xx} & \rho_{x\bar{x}} u^*_{\bar{x}\bar{x}} & \rho_{x\bar{x}} u^*_{\bar{T}\bar{x}} \\ \rho_{\bar{x}x} u_{\bar{x}\bar{x}} & \rho_{\bar{x}\bar{x}} |u_{\bar{x}\bar{x}}|^2 & \rho_{\bar{x}\bar{x}} u^*_{\bar{T}\bar{x}} u_{\bar{x}\bar{x}} \\ \rho_{\bar{x}x} u_{\bar{T}\bar{x}} & \rho_{\bar{x}\bar{x}} u^*_{\bar{x}\bar{x}} u_{\bar{T}\bar{x}} & \rho_{\bar{x}\bar{x}} |u_{\bar{T}\bar{x}}|^2 \end{bmatrix} \equiv \begin{bmatrix} R'_{xx} & R'_{x\bar{x}} & R'_{x\bar{T}} \\ R'_{\bar{x}x} & R'_{\bar{x}\bar{x}} & R'_{\bar{x}\bar{T}} \\ R'_{\bar{T}x} & R'_{\bar{T}\bar{x}} & R'_{\bar{T}\bar{T}} \end{bmatrix}. \quad (39)$$

Note that the expressions in Eq. (39) are in the pulse propagation direction basis, x, and *not* in the energy eigenbasis. We make this choice due to the simplicity of the expressions coming from the optical selection rules. Subsequently, R evolves under the magnetic field and the vacuum radiation field as

$$\dot{R} = i[R, \omega_e S_z] + \mathcal{L}(R). \quad (40)$$

Switching to the interaction picture with respect to the Zeeman Hamiltonian, the following equations describe the evolution of the relevant matrix elements for the 2×2 spin subspace [46],

$$\begin{aligned} \tilde{R}_{xx} &= \gamma R_{\bar{T}\bar{T}}(1 - \cos\omega_e t), \\ \tilde{R}_{\bar{x}\bar{x}} &= \gamma R_{\bar{T}\bar{T}}(1 + \cos\omega_e t), \\ \tilde{R}_{x\bar{x}} &= i\gamma R_{\bar{T}\bar{T}} \sin\omega_e t, \quad \dot{R}_{\bar{T}\bar{T}} = -2\gamma R_{\bar{T}\bar{T}}, \end{aligned} \quad (41)$$

where $\tilde{R}$ is the density matrix in the interaction picture. Equations (41) include the so-called spontaneously generated coherence effect [45–47], which results from the fact that due to polarization selection rules, spontaneous emission couples state $|\bar{T}\rangle$ to $|\bar{x}\rangle$ only [although spontaneous emission *together* with precession leads to some population decaying to $|x\rangle$ as well, as seen in the topmost equation of Eqs. (41)]. This effect is significant when the Zeeman frequency, ω_e, is smaller or comparable to the relaxation rate, γ. From the last equation we readily obtain

$$R_{\bar{T}\bar{T}} = R'_{\bar{T}\bar{T}} e^{-2\gamma t}, \quad (42)$$

which then allows us to find the matrix elements in the spin subspace by a simple integration. Doing that and taking the limit $t \gg \gamma^{-1}$ we find

$$\tilde{R}_{xx} = R'_{xx} + \frac{\omega_e^2}{2(4\gamma^2 + \omega_e^2)} R'_{\bar{T}\bar{T}}, \quad (43)$$

$$\tilde{R}_{\bar{x}\bar{x}} = R'_{\bar{x}\bar{x}} + \left[\frac{2\gamma^2}{4\gamma^2 + \omega_e^2} + \frac{1}{2}\right] R'_{\bar{T}\bar{T}}, \quad (44)$$

$$\tilde{R}_{x\bar{x}} = R'_{x\bar{x}} + i\frac{\gamma\omega_e}{4\gamma^2 + \omega_e^2} R'_{\bar{T}\bar{T}}. \quad (45)$$

Notice that the degree of spin polarization depends on the ratio ω_e/γ, as was discussed in detail in Ref. [46]. In our previous work [39], we considered the high magnetic field limit; i.e., we assumed $\omega_e/\gamma \gg 1$. In that limit Eqs. (43)–(45) above simplify and the coefficients of $R'_{\bar{T}\bar{T}}$ are 1/2 for (43) and (44) and zero for (45). Here we relax that assumption to account for low-B fields.

Combining Eqs. (39) and (43)–(45) we obtain for the spin density matrix in the laboratory frame after the pulse and spontaneous emission

$$\rho'_{xx} = \rho_{xx} + \frac{\omega_e^2}{2(4\gamma^2 + \omega_e^2)} |u_{\bar{T}\bar{x}}|^2 \rho_{\bar{x}\bar{x}}, \quad (46)$$

$$\rho'_{\bar{x}\bar{x}} = \rho_{\bar{x}\bar{x}} |u_{\bar{x}\bar{x}}|^2 + \left[\frac{2\gamma^2}{4\gamma^2 + \omega_e^2} + \frac{1}{2}\right] |u_{\bar{T}\bar{x}}|^2 \rho_{\bar{x}\bar{x}}, \quad (47)$$

$$\rho'_{x\bar{x}} = \rho_{x\bar{x}} u^*_{\bar{x}\bar{x}} + i\frac{\gamma\omega_e}{(4\gamma^2 + \omega_e^2)} |u_{\bar{T}\bar{x}}|^2 \rho_{\bar{x}\bar{x}}, \quad (48)$$

where we have used that $\tilde{\rho}'_{ij} = \rho'_{ij}$. Using the unitarity of U_p, i.e., setting $|u_{\bar{T}\bar{x}}|^2 = 1 - |u_{\bar{x}\bar{x}}|^2$ and by inspection of Eqs. (46)–(48), we obtain the Kraus operators in the laboratory frame (x basis),

$$E_1 = \begin{bmatrix} 1 & 0 \\ 0 & q \end{bmatrix}, \quad E_2 = \begin{bmatrix} 0 & a_1 \\ 0 & -a_2 \end{bmatrix}, \quad E_3 = \begin{bmatrix} 0 & 0 \\ 0 & \kappa \end{bmatrix}, \quad (49)$$

where

$$q = u_{\bar{x}\bar{x}} \equiv q_o e^{i\phi}, \quad (50)$$

$$a_1 = \omega_e \sqrt{\frac{(1 - q_o^2)}{2(4\gamma^2 + \omega_e^2)}}, \quad (51)$$

$$a_2 = i\gamma\sqrt{2}\sqrt{\frac{1 - q_o^2}{4\gamma^2 + \omega_e^2}}, \quad (52)$$

$$\kappa = \sqrt{1 - q_o^2 - a_1^2 - |a_2|^2}. \quad (53)$$

In the limit $\omega_e \gg \gamma$, where the spontaneously generated coherence effect is negligible, we have $a_2 \to 0$ and $a_1, \kappa \to \sqrt{(1 - q_o^2)/2}$, so that we recover the Kraus operators from Ref. [39].

Here it is important to clarify a point of potential confusion. In deriving the above Kraus operators, we assumed $\gamma T_R \gg 1$, so that the trion decays completely back to the electron spin subspace within a single period. Therefore, setting $\gamma = 0$ in the Kraus operators *does not* correspond to the absence of spontaneous emission, but instead it corresponds to neglecting spontaneously generated coherence, i.e., to the case of equal decay to both electron spin states. In what follows, we see that the ratio γ/ω_e plays an important role in the generation of DNP.

The matrix elements of U_p are functions of the pulse-system parameters, namely the Rabi frequency, the detuning, the bandwidth and the pulse shape. For example, in the case where the pulse has the shape of the hyperbolic secant, which is analytically solvable, the matrix element $u_{\bar{x}\bar{x}}$ has the explicit form [54]

$$u_{\bar{x}\bar{x}} = F(a, -a, c^*, 1) = \frac{\Gamma(c)^2}{\Gamma(c - a)\Gamma(c + a)}, \quad (54)$$

where F is Gauss's hypergeometric function, Γ is the Γ function, and $a = \Omega_o/\sigma$ and $c = 1/2(1 + i\Delta/\sigma)$, with Ω_o, Δ, and σ denoting the Rabi frequency, pulse detuning, and bandwidth, respectively. In this case, the Kraus parameter q_o can be expressed as

$$q_o = |u_{\bar{x}\bar{x}}| = \sqrt{1 - \sin^2(\pi\Omega_o/\sigma)\mathrm{sech}^2(\pi\Delta/2\sigma)}. \quad (55)$$

In principle, q_o and ϕ can be computed for any pulse shape; thus we continue to express results in terms of these parameters for the sake of generality.

The quantities q_o and ϕ are two of the key parameters of the theory. Physically, $1 - q_o^2$ is the fraction of population that moves from the electron spin state $|\bar{x}\rangle$ to the trion state $|\bar{T}\rangle$, while ϕ is the angle about the x axis by which the pulse rotates the electron spin, with its sign coinciding with that of the detuning, Δ.

B. Electron and nuclear spin steady states and nuclear relaxation rate

Transforming the Kraus operators of Eq. (49) to the z basis and using Eqs. (13) and (14), we find

$$K_e = \begin{bmatrix} a_1^2 & -ia_1a_2 & 0 \end{bmatrix}, \qquad Y_e = \begin{bmatrix} 1-a_1^2 & 0 & 0 \\ ia_1a_2 & q_o\cos\phi & -q_o\sin\phi \\ 0 & q_o\sin\phi & q_o\cos\phi \end{bmatrix}. \quad (56)$$

Combining these results with the evolution operator describing precession between pulses,

$$Y_{pr} = \begin{bmatrix} \cos(\omega_e T_R) & -\sin(\omega_e T_R) & 0 \\ \sin(\omega_e T_R) & \cos(\omega_e T_R) & 0 \\ 0 & 0 & 1 \end{bmatrix}, \quad (57)$$

we obtain the electron steady state right after each pulse from the formula, $S_e^{(\infty)} = (1 - Y_e Y_{pr})^{-1} K_e$, with

$$S_{e,x}^{(\infty)} = \frac{a_1[a_1q_o(q_o - \cos\phi)\cos(\omega_e T_R) - ia_2(q_o\cos\phi - 1)\sin(\omega_e T_R) - a_1q_o\cos\phi + a_1]}{(a_1^2 + q_o^2 - 1)\cos(\omega_e T_R) - a_1q_o\cos\phi[ia_2\sin(\omega_e T_R) + a_1\cos(\omega_e T_R) + a_1] + ia_1a_2\sin(\omega_e T_R) + (a_1^2 - 1)q_o^2 + 1},$$

$$S_{e,y}^{(\infty)} = \frac{a_1(a_1q_o(\cos\phi - q_o)\sin(\omega_e T_R) - ia_2(q_o\cos\phi - 1)[\cos(\omega_e T_R) - 1])}{(a_1^2 + q_o^2 - 1)\cos(\omega_e T_R) - a_1q_o\cos\phi[ia_2\sin(\omega_e T_R) + a_1\cos(\omega_e T_R) + a_1] + ia_1a_2\sin(\omega_e T_R) + (a_1^2 - 1)q_o^2 + 1},$$

$$S_{e,z}^{(\infty)} = \frac{a_1q_o\sin\phi(a_1\sin(\omega_e T_R) - ia_2(\cos(\omega_e T_R) - 1))}{(a_1^2 + q_o^2 - 1)\cos(\omega_e T_R) - a_1q_o\cos\phi[ia_2\sin(\omega_e T_R) + a_1\cos(\omega_e T_R) + a_1] + ia_1a_2\sin(\omega_e T_R) + (a_1^2 - 1)q_o^2 + 1}. \quad (58)$$

Note that the steady state undergoes Larmor precession during each period and that the state at any point during the period can be obtained by evolving the above expressions using Eq. (57).

At this point it is useful to verify the separation of time scales necessary for the validity of the Markovian approximation discussed in Sec. V D. In particular, we want to show that the time it takes for the electron spin to reach this steady state, which we define as τ_e, is small compared to the typical decoherence time. As in the case of the nuclear spin (discussed in Sec. V D), we can obtain τ_e from the eigenvalues of $\mathbb{1} - \mathcal{Y}_e$. In the special case of resonant π pulses, $q_o = 0$, we obtain the analytical expression

$$\tau_e = \frac{2T_R(\omega_e^2 + 4\gamma^2)}{2(\omega_e^2+4\gamma^2) - (\omega_e^2+8\gamma^2)\cos(\omega_e T_R) + 2\gamma\omega_e\sin(\omega_e T_R)}.$$

From this expression, it is clear that the slowest relaxation times occur when the frequency is commensurate with the pulse train period. In that case we obtain $\tau_e \to (2 + 8\gamma^2/\omega_e^2)T_R$. We have also checked that a similar time scale holds for other values of $q_o \lesssim 0.5$. In Fig. 2 we plot the SV components as functions of the coarse-grained time for $q_0 = 0.3$ and also show the trend for the coarse-grained evolution of the electron spin x component as a function of q_o. From these figures, it is evident that the electron spin reaches its steady state after only a few periods. For typical pulse periods $T_R \sim 10$ ns, we have $\tau_e \lesssim 100$ ns, which is well below typical decoherence times of several microseconds, justifying the use of a Markovian approach. For values of $q_o \gtrsim 0.5$, it is apparent from the bottom panel of Fig. 2 that the electron spin reaches its steady state sufficiently slowly that the validity of the Markovian approach is questionable. This highlights the intrinsic connection between the smallness of q_o and Markovianity, which was pointed out in Ref. [39]. For the numerical results we present below, we use $q_o = 0.3$, a value which is both well within the Markovian regime and also large enough that coherent effects due to the pulses are significant.

C. Nuclear steady state and relaxation rate

Given expressions (58) for the electron steady state, we can compute the nuclear spin steady state and relaxation rate from Eqs. (27) and (28). The nuclear relaxation rate $\gamma_n = \lambda_2^*/T_R$ is shown in Figs. 3(a) and 3(b) as a function of the electron Zeeman energy. It is apparent from the figures that this rate becomes larger as the Zeeman energy decreases. This trend is due to the fact that the electron spin flips more easily with nuclear spins when its Zeeman energy is smaller, leading to faster relaxation. Figures 3(c)–3(f) reveal that this feature of γ_n carries over to the difference of the single-nucleus spin flip rates, $w_\pm$, even though the nuclear steady state is larger at higher magnetic fields. As we see in the next section, this difference in flip rates leads to a nonzero average nuclear spin polarization at lower magnetic fields. Note that in Fig. 3, we have taken the rotation angle to be $\phi = -\pi/2$. Reversing the sign of ϕ changes the sign of $S_{e,z}^{(\infty)}$ and hence the sign of $w_+ - w_-$. Thus, the sign of

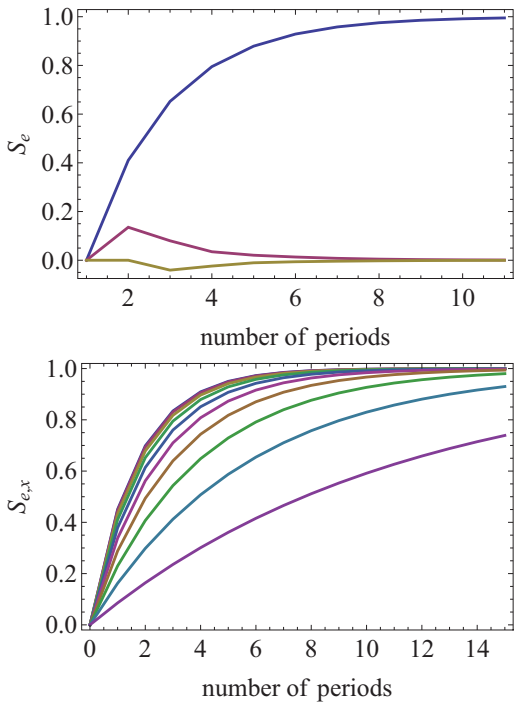

FIG. 2. (Color online) Coarse-grained electron spin evolution for $T_R = 13.2$ ns, $\gamma = 0.5$ GHz, $\phi = -\pi/2$. (Top) All three components (lines, top to bottom: $S_{e,x}, S_{e,y}, S_{e,z}$) for $q_o = 0.3$; (bottom) $S_{e,x}$ for $q_o = 0, 0.1, \ldots, 0.9$ (lines, top to bottom).

the nuclear spin polarization depends directly on the sign of ϕ.

It is also apparent from Fig. 3 that γ_n and hence the flip-rate difference periodically go to zero. This behavior stems directly

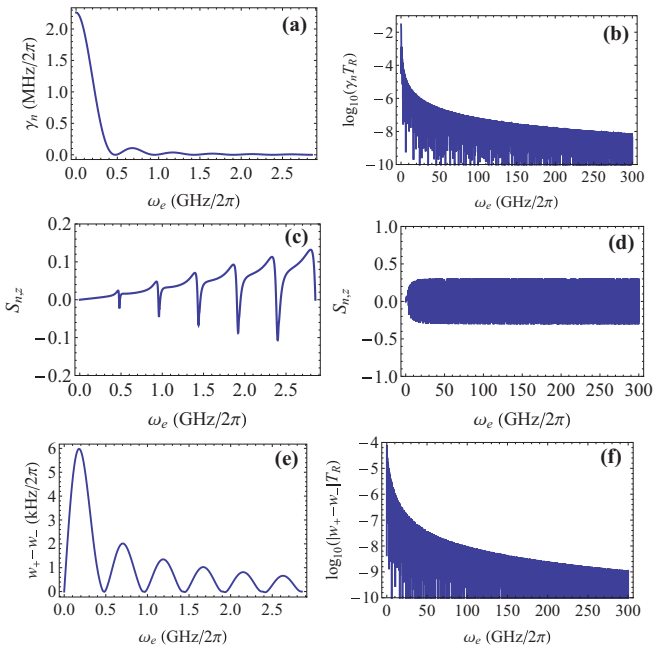

FIG. 3. (Color online) (a), (b) Nuclear relaxation rate, (c), (d) steady state, and (e), (f) difference of single-nucleus flip rates versus electron Zeeman energy for $T_R = 13.2$ ns, $NA = 12.5$ GHz, $N = 3000$, $\gamma = 0.5$ GHz, $q_0 = 0.3$, $\phi = -\pi/2$, $\omega_n = 0$. The expression (GHz/2π) in the units of ω_e is equivalent to radians per nanosecond.

from the sine factor in Eq. (28), which vanishes when the Zeeman precession period is commensurate with the pulse period. When this condition is satisfied, the electron spin is polarized along the x direction when the pulse arrives and is thus unaffected by the pulses, removing the mechanism through which the nuclear spin attains its steady state and leading to $\gamma_n = 0$. This feature of γ_n plays a central role in the frequency focusing effect, as is explained in the next section.

It should be mentioned that since the results shown in Fig. 3 were obtained using a perturbation theory that assumes $A/\omega_e \gg 1$, we cannot trust the results for values of ω_e very close to zero. For the parameters used in the plots, this implies that perturbation theory is valid for $\omega_e \gg 0.026$ rad/ns. This condition should also be kept in mind below when we include the Overhauser shift to obtain the effective electron Zeeman frequency, which must satisfy the same condition. For the external magnetic fields we consider and Overhauser shifts we calculate, this condition is satisfied for all the results we obtain in the paper.

D. Incorporating multinuclear effects: Self-consistent Overhauser shift

Using the flip rates for a single nuclear spin obtained in the previous section, we shift the electron Zeeman frequency by the Overhauser field as described by Eq. (34) to obtain flip rates that take into account the effect of the full nuclear spin bath. We then feed these flip rates into the recurrence relation, Eq. (35), that defines the steady-state solution of the nuclear polarization rate equation (33). We solve this recurrence relation numerically for small ($B = 0.1$ T) and large ($B = 6$ T) values of the magnetic field and for three different values of the pulse rotation angle ϕ ($0, \pm\pi/2$). We choose the electron g factor to be such that $\omega_e/B = 7.14$ GHz/T, so that the two values of B we consider correspond to $\omega_e = 4.5$ rad/ns and $\omega_e = 269.2$ rad/ns. The results are shown in Fig. 4.

Each panel of the figure clearly shows that the polarization distribution generally exhibits a series of equally spaced peaks. The spacing is given by $\Delta m = 4/(AT_R)$ and is a direct manifestation of the frequency focusing phenomenon described in Ref. [4] in which the nuclear polarization builds up in such a way as to shift the electron Zeeman frequency to values commensurate with the pulse frequency. In particular, the polarization peaks are located at values of m such that $(\omega_e + Am/2)T_R$ is an integer multiple of 2π. The physics leading to this effect is as follows: An electron spin with Zeeman frequency $\omega_e \neq 2\pi n/T_R$ will undergo dynamics that cause the nuclear spins to flip; see Eq. (28). Through this process, the Overhauser shift will alter the dynamics of the electron spin itself, until the shifted electron Zeeman frequency satisfies the relation $\omega_e = 2\pi n/T_R$, at which point the process stops since the nuclear spin flip rates vanish at these values of ω_e. Therefore, there is a tendency for the system to synchronize with the pulses, leading to the sharp, equally spaced peaks of Fig. 4. This comblike structure can, in fact, be derived analytically by taking the continuum limit of the kinetic equation, as shown in Appendix E. While the variance of the full distribution is comparable to that of a thermal state, each peak is substantially narrower, and this should lead to longer coherence times for the electron spin.

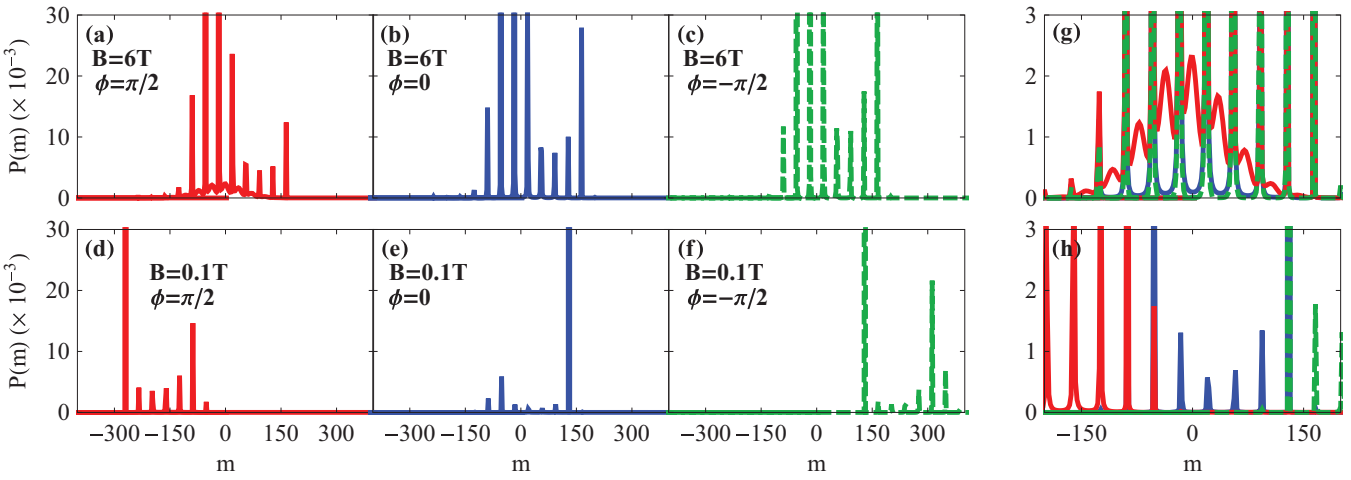

FIG. 4. (Color online) (a)–(f) Nuclear spin polarization distribution for $T_R = 13.2$ ns, $NA = 12.5$ GHz, $N = 3000$, $\gamma = 0.5$ GHz, $q_o = 0.3$, $\omega_n = 0$ for various magnetic fields and rotation angles. Note that several of the peaks extend well beyond the vertical range displayed. (g) Magnification of (a), (b), (c). (h) Magnification of (d), (e), (f).

This focusing effect arises directly from the sine factor in Eq. (28) and is independent of whether w_+ is larger or smaller than w_-. However, this effect can either be enhanced or reduced depending on the behavior of $w_+ - w_-$ in the vicinity of the synchronization points:

$$w_+ - w_- = \gamma_n(2\pi n/T_R + \delta\omega_e)S^{(\infty)}_{n,z}(2\pi n/T_R + \delta\omega_e)$$
$$\approx \frac{A^2 T_R^4 q_o \sin\phi}{8\pi^2\left(1 + q_o^2 - 2q_o\cos\phi\right)}\delta\omega_e^3. \quad (59)$$

Consider first the case $\phi < 0$. In this case, when $\delta\omega_e > 0$, we have $w_+ < w_-$, so that there is a tendency to generate negative nuclear polarization. This negative polarization will shift ω_e toward smaller values via the Overhauser shift. On the other hand, when $\delta\omega_e < 0$, we have $w_+ > w_-$, and positive polarization is produced, shifting ω_e toward larger values. Thus, we see that when $\phi < 0$, the commensurate values $\omega_e = 2\pi n/T_R$ are stable fixed points, and nuclear polarization forms in such a way as to drive the effective electron Zeeman frequency toward these values, further enhancing the sharp, evenly spaced peaks in Fig. 4. This enhancement is particularly evident in the feedback effect on the electron spin that will be examined in the next section.

When $\phi > 0$, we have the reverse situation, where now positive deviations $\delta\omega_e > 0$ lead to positive polarization and negative deviations to negative polarization. Therefore, in this case, the commensurate values $\omega_e = 2\pi n/T_R$ become unstable fixed points, with a nuclear polarization-driven repulsion of the effective ω_e away from these points. This "antisynchronization" effect is evident in Figs. 4(a) and 4(g), where the curve corresponding to $\phi = \pi/2$ exhibits additional, broad peaks centered between the narrow peaks. This effect was first studied theoretically and experimentally in Ref. [40]. In this regime, one might be tempted to say that there exists a stable stationary state between two adjacent, repulsive commensurate points; however, such a state would only be approximately stationary. This is because the nuclear spin-flip rates are nonzero for all values of the electron Zeeman frequency between the two commensurate points, implying that the state continues to evolve. Since this evolution is constrained by the two repulsive fixed points, we envision the state as going back and forth between them, such that the system spends more time at the half-commensurate points on average, leading to an approximate stationary state there. This is to be contrasted with the truly stable fixed points that occur at the commensurate values when $\phi < 0$. At these points, the nuclear flip rates are precisely zero, signifying a real stationary state. Both synchronization and antisynchronization peaks appear in Fig. 4(a) since the ϕ-independent focusing effect in which nuclear spin fluctuations randomly shift the electron Zeeman frequency to commensurate values is still present.

It is also apparent from Fig. 4 that the polarization distribution $P(m)$ is centered around nonzero polarizations when $B = 0.1$ T and ϕ is nonzero. Figure 4 further reveals that the sign of the net polarization that occurs at low magnetic fields is opposite to the sign of ϕ, as was anticipated in the previous section. The values $\phi = \pm\pi/2$ chosen for the figure give rise to maximal values for the polarization; the magnitude of the polarization increases steadily up to $\phi = \pm\pi/2$, and beyond these values, the polarization steadily decreases, returning to values close to zero at $\phi = \pm\pi$. In Fig. 4, it is also clear that the net polarization is significantly reduced at large magnetic fields even for $\phi = \pm\pi/2$. This trend is more explicit in Fig. 5, where we plot the average nuclear polarization, $\bar{m} = \sum_m m P(m)$, as a function of magnetic field. This figure shows that the DNP is largest at low magnetic fields and is suppressed at high magnetic fields. This behavior originates from the phenomenon of spontaneously generated coherence, which are discussed in detail in Sec. VI F.

E. DNP feedback on electron spin

Having calculated the nuclear spin distribution, we proceed to find the feedback on the electron steady state. The total nuclear polarization shifts the Zeeman frequency of the electron spin, and the features of the nuclear distribution described in the previous section are therefore anticipated to appear

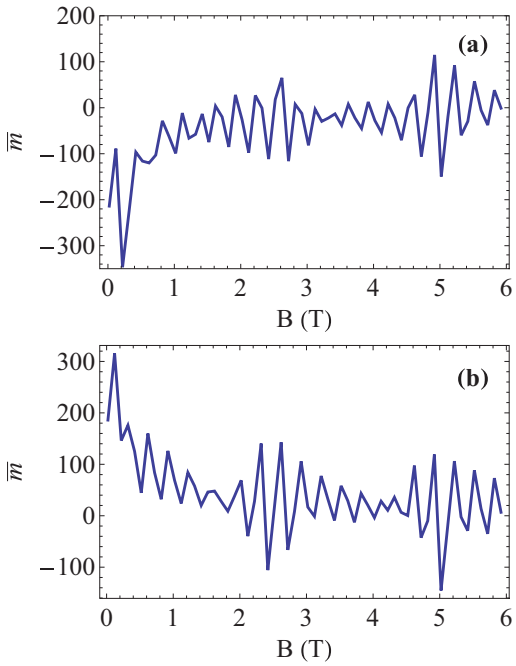

FIG. 5. (Color online) Average nuclear spin polarization versus magnetic field for $T_R = 13.2$ ns, $NA = 12.5$ GHz, $N = 3000$, $\gamma = 0.5$ GHz, $q_o = 0.3$, $\omega_n = 0$, and (a) $\phi = \pi/2$, (b) $\phi = -\pi/2$.

in the final electron spin steady state. Using the expressions for the electron spin components, Eqs. (58), we average ω_e over the distribution $P(m)$, as explained in Sec. V H. The resulting electron SV is shown without and with feedback for $\phi = 0$ in Fig. 6, and for $\phi = \pm\pi/2$ in Fig. 7. From these figures it is evident that the SV components oscillate rapidly as functions of magnetic field and that the amplitude of these oscillations is dramatically reduced when nuclear feedback is included. Furthermore, we see that the x component of the electron SV tends to 1, while the y,z components tend to 0. This shows that the nuclear polarization is built up in such

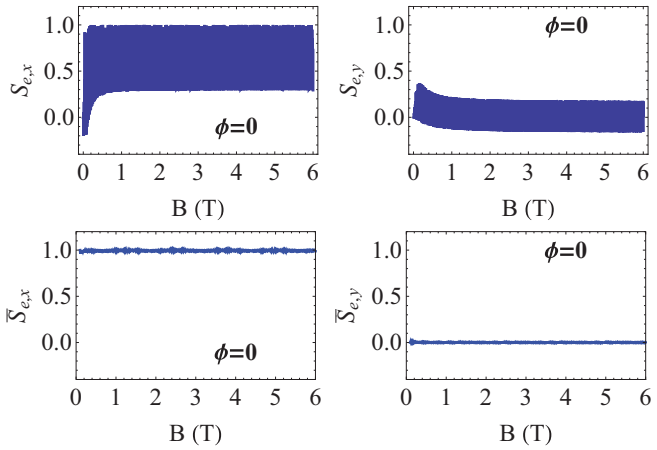

FIG. 6. (Color online) Effect of nuclear feedback. Electron spin steady state versus magnetic field for $T_R = 13.2$ ns, $NA = 12.5$ GHz, $N = 3000$, $\gamma = 0.5$ GHz, $q_o = 0.3$, $\omega_n = 0$, $\phi = 0$. (Top panels) Without nuclear feedback [Eq. (58)]; (bottom panels) with nuclear feedback [Eq. (36)].

a way that it synchronizes the electron spin with the pulse so that its steady state at the time of the pulse is now fully polarized along x. Note also the effect of synchronization and antisynchronization (discussed in the previous section) in the SV components. The nuclear feedback in both cases focuses the electron Zeeman splitting through synchronization, but in the case of $\phi = \pi/2$ the effect is weaker. This can be seen more clearly in Fig. 8, where we have magnified the spin components for all three cases, $\phi = 0, \pm\pi/2$, revealing an increasing synchronization effect as we move from positive to negative ϕ. In particular, we see that in the case of positive ϕ the amplitude of oscillation of the $S_{e,x}$ component is significantly larger as compared to zero and negative ϕ's.

F. Effects of spontaneously generated coherence

As mentioned above, our solution is valid throughout the full range of magnetic field values, including the low magnetic field regime, which was beyond the scope of our earlier work [39]. This is achieved by taking fully into account the phenomenon of spontaneously generated coherence (SGC), which is present in these QDs and is most prominent at low magnetic fields. The effect of SGC, first predicted theoretically in the early 1990s [45] and about a decade later investigated theoretically [46] and experimentally [47] in the context of optically controlled QDs, amounts to a coherence term in the decay equations driven by the spontaneous emission from the excited level. Though this may seem counterintuitive at first, it is not difficult to understand if we consider the limiting case of zero magnetic field in our system. In that case, the only decay process is from state $|\bar{T}\rangle$ to $|\bar{x}\rangle$ both in the laboratory and in the rotating frame. Equations (41) then reduce to a single nontrivial equation,

$$\dot{R}_{\bar{x}\bar{x}} = \tilde{\dot{R}}_{\bar{x}\bar{x}} = 2\gamma R_{\bar{T}\bar{T}}. \tag{60}$$

This reflects the fact that in the $B = 0$ limit, state $|x\rangle$ is completely decoupled from the dynamics. When the field is switched on, Eq. (60) still holds in the laboratory frame, and the additional terms in Eqs. (41) arise from the transformation to the rotating frame. We can understand intuitively the origin of the SGC term from the fact that population terms in one basis give rise to coherence terms in a different basis. Thus, in the magnetic field basis z, the term $R_{\bar{x}\bar{x}}$ is a linear combination of all four population and coherence terms R_{ij} with $i,j = |z\rangle, |\bar{z}\rangle$. Therefore, there is a coherence term generated by spontaneous emission. This effect is independent of basis, and in the x basis and rotating frame, it can be expressed as a coherence between states $|x\rangle$ and $|\bar{x}\rangle$, as seen in Eqs. (41).

To discuss the effects this term has on the nuclear dynamics, it is useful to first think of the effect on the electron spin alone as compared to the absence of SGC. This was already discussed at length in Ref. [46], but it is worth summarizing that discussion here for the sake of completeness. First, by inspecting the decay equations and their solutions, we can immediately see that SGC has the tendency to create electron spin polarization along the $+y$ axis. This can also be seen through a geometric picture of the spin as follows.The pulse removes part of the SV pointing along $-x$ (how much depends on q_o). The SV that remains along x precesses about the z axis counterclockwise. For concreteness, consider a mixed initial

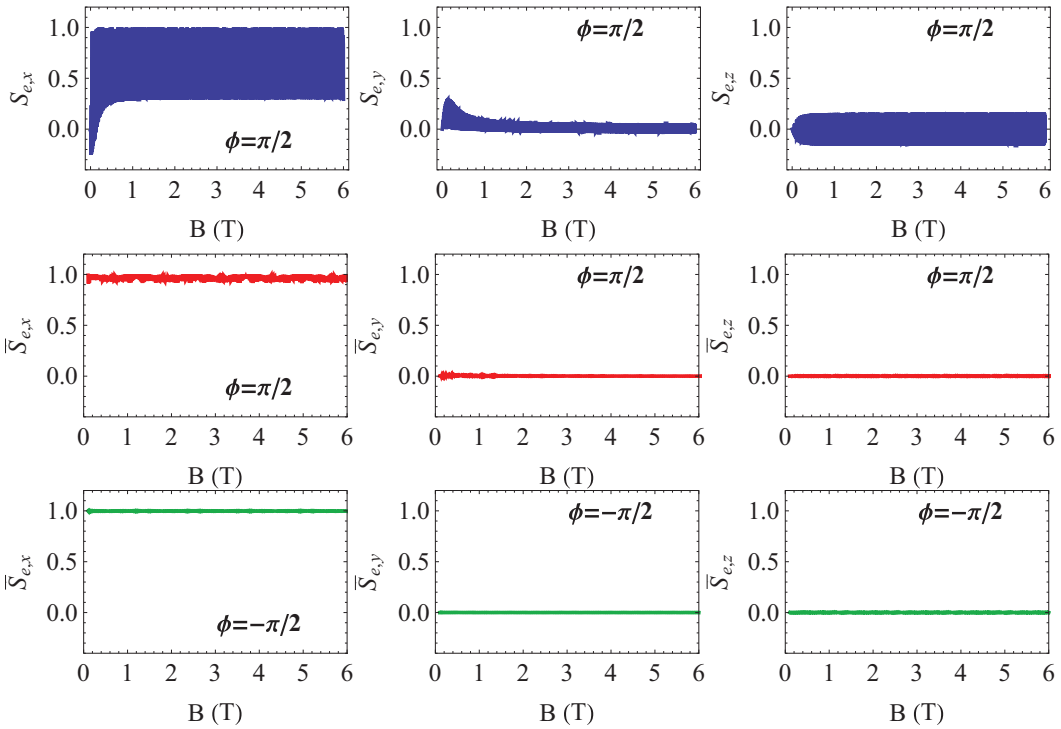

FIG. 7. (Color online) Effect of nuclear feedback. Electron spin steady state versus magnetic field for $T_R = 13.2$ ns, $NA = 12.5$ GHz, $N = 3000$, $\gamma = 0.5$ GHz, $q_o = 0.3$, $\omega_n = 0$. (Top row) Without nuclear feedback [Eq. (58)] for $\phi = \pi/2$ (the case with $\phi = -\pi/2$ is essentially the same); (middle row) with nuclear feedback [Eq. (36)] for $\phi = \pi/2$; (bottom row) with nuclear feedback [Eq. (36)] for $\phi = -\pi/2$.

state and a pulse that is close to π, i.e., $q_o \sim 0$. There is then a net SV component pointing along $+x$ which begins to precess toward $+y$. As the spontaneous emission occurs, it can be thought of as contributing small vectors that point toward $-x$, adding on to the "unexcited" part of the SV, which is now in the $x, y > 0$ quadrant. This process continues until

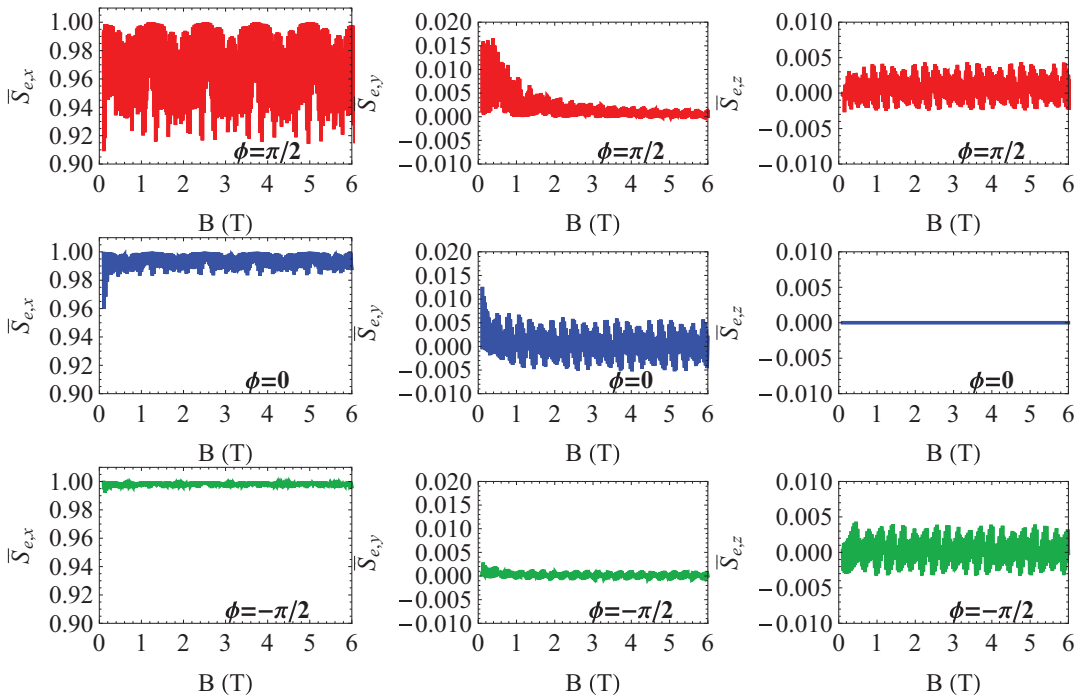

FIG. 8. (Color online) Effect of nuclear feedback. Magnification of electron spin steady state versus magnetic field including nuclear feedback for $T_R = 13.2$ ns, $NA = 12.5$ GHz, $N = 3000$, $\gamma = 0.5$ GHz, $q_o = 0.3$, $\omega_n = 0$ for the three cases, $\phi = 0, \pm\pi/2$. In the case $\phi = \pi/2$, the antifocusing effect is evident in the x component of the electron steady state, while the case $\phi = \pi/2$ gives stronger focusing compared to the $\phi = 0$ case.

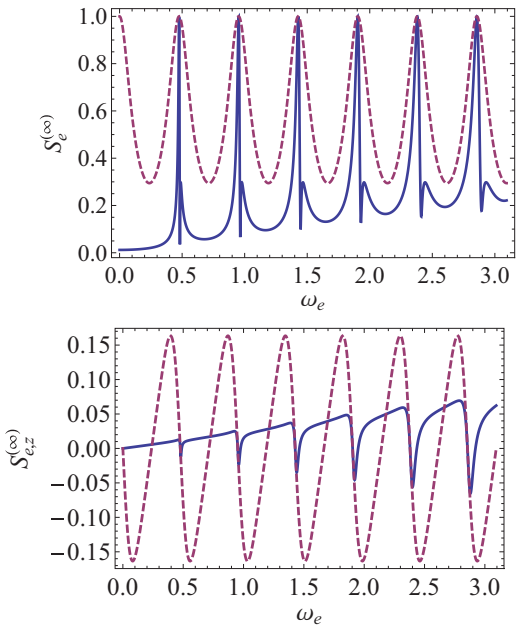

FIG. 9. (Color online) Checking the effect of SGC. Total electron steady-state SV (top panel) and z component (bottom panel) for $T_R = 13.2$ ns, $\phi = -\pi/2$, and $\gamma = 0.5$ GHz (solid), $\gamma = 0$ (dashed). For $\gamma = 0$, there is no SGC.

the excited state has fully decayed. The spontaneous emission in this case partially opposes the generation of coherence by adding a coherent component along $-x$. However, the spin component that is pointing along y is "protected," and thus in the rotating frame we can think of a net y component created by the total process of excitation and spontaneous emission including SGC.

The situation is more complicated when the pulse, in addition to polarizing/depolarizing the SV, also rotates the spin. This is the case when $q_o \neq 0, \phi \neq 0$. The rotation is about the x axis, so that the y component of the SV due to SGC is rotated to z. As a result, there is a persistent z component of the SV in the general case when both SGC and the pulse-induced rotation are considered. This effect is evident in the asymmetric form of the z component shown in Fig. 9. The z component of the nuclear spin is itself a monotonically increasing function of the electron spin z component [Eq. (27)]. Therefore, SGC has the effect of creating more nuclear polarization along z on average, which in turn controls the relative size of the nuclear spin-flip rates in the two directions (up to down vs down to up). We therefore expect this to translate into a larger nuclear spin polarization relative to the case of no SGC, which is what we see when we compare Figs. 4, 5 and 10, 11.

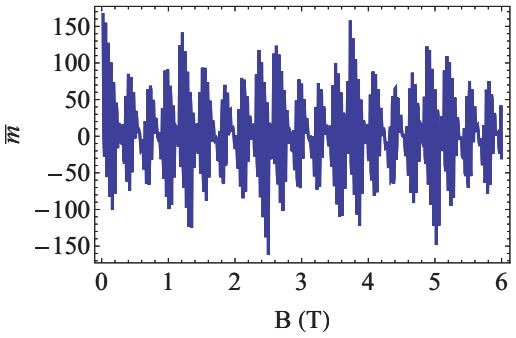

FIG. 11. (Color online) Checking the effect of SGC. Average nuclear spin polarization versus magnetic field for $T_R = 13.2$ ns, $NA = 12.5$ GHz, $N = 3000$, $\gamma = 0$, $q_o = 0.3$, $\omega_n = 0$, and $\phi = \pi/2$.

G. Spin echo

We now examine how the nuclear feedback mechanism is altered by the addition of an extra, unitary pulse in the middle of each period, i.e., at a time interval $T_R/2$ from the nonunitary pulse of the sequence. We specifically choose this additional pulse such that it implements a π rotation of the electron spin around the x axis. This can therefore be thought of as a spin-echo sequence and the pulse as an echo pulse. It is straightforward to include this pulse into our formalism by replacing the unitary part of the evolution $U_{hf}(T_R)$ between pulses with

$$U_{hf}(T_R/2)[R_x(\pi) \otimes \mathbb{1}]U_{hf}(T_R/2), \tag{61}$$

where $R_x(\pi) = e^{-i\pi s_1}$ denotes the spin rotation implemented by the echo pulse. In this case, the steady state of the electron spin turns out to be

$$S_e^{SE} = (1,0,0). \tag{62}$$

This steady state coincides with that of the synchronized spins in the absence of the echo pulse, so one may be tempted to think that the dynamics is trivial in the spin-echo case and that no nuclear dynamics occurs. This is, in fact, false; the nuclear dynamics and subsequent feedback mechanism turn out to be distinct and interesting in the presence of spin echo.

Following the same steps outlined in Appendix A, we find that the nuclear spin steady state is trivial, $S_n^{(\infty)} = (0,0,0)$,

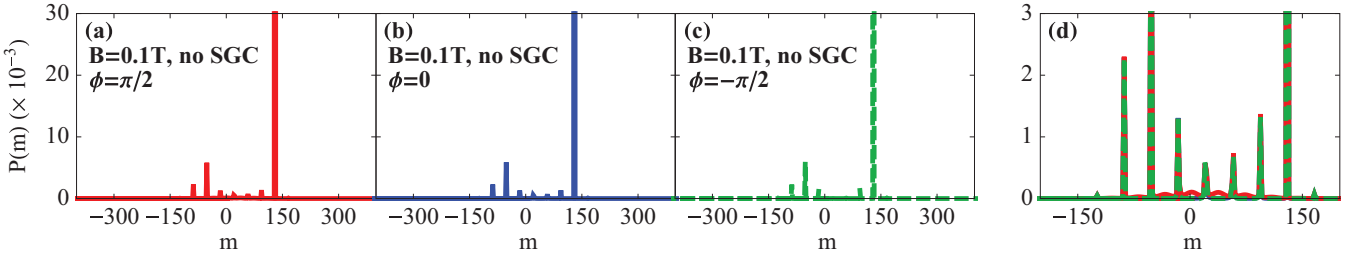

FIG. 10. (Color online) Checking the effect of SGC. (a)–(c) Nuclear spin polarization distribution for $T_R = 13.2$ ns, $NA = 12.5$ GHz, $N = 3000$, $\gamma = 0$, $q_o = 0.3$, $\omega_n = 0$, $B = 0.1$ T for various rotation angles. (d) Magnification of (a),(b),(c).

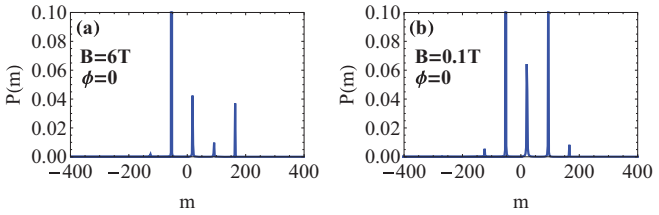

FIG. 12. (Color online) Effect of spin-echo pulse. Nuclear spin polarization distribution for $T_R = 13.2$ ns, $NA = 12.5$ GHz, $N = 3000$, $\gamma = 0.5$ GHz, $q_o = 0.3$, $\omega_n = 0$, $\phi = 0$, and (a) $B = 6$ T, (b) $B = 0.1$ T.

while the nuclear spin-flip rates are

$$\mathrm{w}_+ = \mathrm{w}_- = \frac{A^2 \sin^2(\omega_e T_R/4)}{\omega_e^2 T_R}. \tag{63}$$

This result clearly differs from what would be obtained from Eqs. (27), (28), and (31) if we were to set $S_e = (1,0,0)$, with perhaps the most striking difference being the extra factor of $1/2$ in the argument of the sine. This indicates that the synchronized electron Zeeman frequencies are no longer given by $2n\pi/T_R$ but instead by $4n\pi/T_R$. The physical origin of this is that the evolution of the electron-nuclear spin entanglement is modified by the echo pulse, and in particular it is no longer the case that spins become disentangled after a time span of $2\pi/\omega_e$; instead, this disentanglement occurs after a time interval of $4\pi/\omega_e$. Therefore, if the nonunitary pulse is applied at time $t = 2\pi/\omega_e$, the residual entanglement will polarize the nuclear spin, whereas if it is applied at $t = 4\pi/\omega_e$, no polarization is produced.

Using the rates from Eq. (63), we calculate the nuclear spin polarization distribution, and the results are shown in Fig. 12. As in the case without the echo pulse, we find that the distribution exhibits a sequence of equally spaced peaks, this time with a spacing period of $\Delta m = 8/(AT_R)$, twice as large as without echo. These peaks again indicate a focusing effect, this time at the spin-echo-synchronized Zeeman frequencies, $4n\pi/T_R$. Since $\mathrm{w}_+ = \mathrm{w}_-$ regardless of the value of ϕ or any other parameters, the physics of this focusing effect is analogous to the $\phi = 0$ case in the absence of spin echo. The equality of the flip rates also means that the net nuclear spin polarization is minimal, as shown in Fig. 13. The fact that $\mathrm{w}_+ = \mathrm{w}_-$ allows for an explicit analytical solution of the polarization distribution in the continuum limit, as shown in Appendix E.

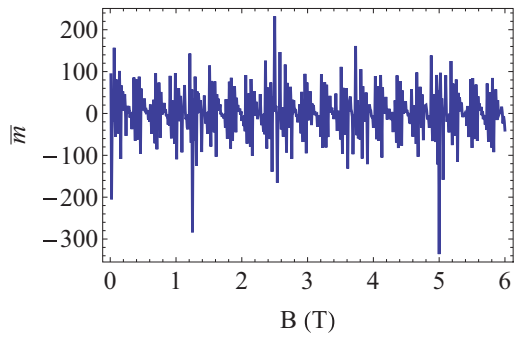

FIG. 13. (Color online) Effect of spin-echo pulse. Average nuclear spin polarization distribution versus magnetic field for $T_R = 13.2$ ns, $NA = 12.5$ GHz, $N = 3000$, $\gamma = 0.5$ GHz, $q_o = 0.3$, $\omega_n = 0$, $\phi = 0$.

VII. CONCLUSIONS AND OUTLOOK

The field of nuclear spin control via the combination of coherent and incoherent driving of an electron spin confined in a QD, while very vibrant and rapidly growing, is still at an early stage regarding a microscopic understanding of the key fundamental processes that occur in these systems. In this work, we presented a general formalism to treat the generation of DNP and its feedback effects on the electron spin both microscopically and self-consistently. Although these experiments are quite complex, we showed that by taking advantage of the separation of time scales that typically occur in these experimental setups and by employing powerful techniques from the field of quantum information, the theoretical description cannot only be rendered tractable but can yield analytical results that permit greater insight into the underlying physics. In particular, our formalism reveals the crucial role of electron-nuclear entanglement in the formation of DNP.

Our theory can be adapted, in principle, to any experimental setup where the electron is driven while interacting with the nuclear bath and with an additional reservoir. To demonstrate our theoretical framework, in this paper we analyzed in detail the mode-locking experiments in which the electron spin is driven by a periodic train of fast circularly polarized laser pulses. We showed that our theory reproduces the main signatures of DNP in these experiments, namely the synchronization and antisynchronization of the electron spin precession with the pulse repetition rate. Furthermore, our formalism predicts an enhancement of DNP at lower external magnetic fields due to the phenomenon of SGC, an effect that was not included in previous treatments of the nuclear spin/DNP problem. In addition, we applied our theory to the case where an extra spin-echo pulse is inserted between every adjacent pair of mode-locking pulses; this insertion constitutes the simplest implementation of dynamical decoupling in these experiments. Our results predict that the inclusion of the spin-echo pulse both modifies the synchronization condition and significantly reduces the amount of DNP generated.

In this work we made certain assumptions and approximations. First and foremost, we exploited the separation of time scales in this problem, which enabled a Markovian approach. We argued that because processes leading to electron spin decoherence were ignored, the Markovian approximation here was actually *more* appropriate compared to a non-Markovian treatment in which the full electron-nuclear spin correlations are retained. This is because the decoherence is fast compared to nuclear spin dynamics, implying that such correlations will decay before they become significant. Moreover, since the electron spin reaches its dynamical steady state quickly compared to the decoherence time scale, the electron will tend to remain in its steady state on average. These observations together suggest that the primary source of DNP feedback on the electron spin is through a modification of its precession frequency due to the Overhauser field of the nuclear spins; this is the type of feedback we have focused on in this work.

A complete treatment of the full dynamics of this problem would entail going beyond the Markovian limit by properly taking into account electron spin decoherence at a microscopic level. If this could be done, it would constitute an important breakthrough as it would lead to a formalism capable of describing any DNP experiment in QDs. However, this is a challenging problem as it would require abandoning the independent-nucleus approximation and including the full effect of the nuclear spin ensemble in the calculation of the electron spin steady state. Going beyond the independent-nucleus approximation would also allow us to investigate the role of internuclear spin entanglement in the generation of DNP and in nuclear feedback effects. A promising approach to achieve this would be to incorporate techniques from the theory of generalized master equations [53] into our formalism. These techniques are similar in spirit to the operator sum representation employed in this work in that they can offer a dramatic reduction in the effective size of the Hilbert space without invoking additional assumptions or approximations. We leave the development and exploration of this more complete theoretical formalism to future work.

ACKNOWLEDGMENTS

We thank S. Carter and E. N. Economou for their careful reading of the manuscript and useful comments. This work was supported by LPS-CMTC (E.B.) and in part by ONR (S.E.E.).

APPENDIX A: NUCLEAR SPIN STEADY STATE AND RELAXATION RATE FROM PERTURBATION THEORY

As discussed in Sec. V E, we can obtain analytical expressions for the nuclear spin steady state and relaxation rate by performing a perturbative expansion in the hyperfine flip-flop interaction (retaining the Overhauser part of the interaction to all orders). The first step is to expand $\mathcal{Y}_n$ in powers of the hyperfine flip-flop interaction:

$$\mathcal{Y}_n = \mathcal{Y}_n^{(0)} + \mathcal{Y}_n^{(1)} + \mathcal{Y}_n^{(2)} + \cdots . \tag{A1}$$

A similar expansion can be performed for the effective 4D SV of the nucleus:

$$\mathcal{S}_n = \mathcal{S}_n^{(0)} + \mathcal{S}_n^{(1)} + \mathcal{S}_n^{(2)} + \cdots . \tag{A2}$$

The goal of this appendix is to derive a formula for the nuclear spin relaxation rate and zeroth-order steady state in terms of the first three terms in the expansion of $\mathcal{Y}_n$ [Eq. (A1)]. The key observation that facilitates this derivation is that to zeroth order in the flip-flop term, the evolution of the nuclear spin is simple precession, at most modified by the effective magnetic field due to the electron spin component along the z axis (the so-called Knight field). Thus, $\mathcal{Y}_n^{(0)}$ will have the general form

$$\mathcal{Y}_n^{(0)} = \begin{bmatrix} 1 & 0 & 0 & 0 \\ 0 & \mathcal{Y}_{n,xx}^{(0)} & \mathcal{Y}_{n,xy}^{(0)} & 0 \\ 0 & \mathcal{Y}_{n,yx}^{(0)} & \mathcal{Y}_{n,yy}^{(0)} & 0 \\ 0 & 0 & 0 & 1 \end{bmatrix}. \tag{A3}$$

Here the first row is (1,0,0,0) because this is generally the case for an evolution operator in the 4D SV representation. The first column is (1,0,0,0) because no polarization is generated; the nuclear spin evolution is unitary at zeroth order. The remaining 3×3 submatrix implements (modified) precession in the xy plane. It will turn out that this generic form is already sufficiently restricted that we can make substantial progress without specifying the explicit expressions for the $\mathcal{Y}_{n,xx}^{(0)}$, etc., or for $\mathcal{Y}_n^{(1)}$ and $\mathcal{Y}_n^{(2)}$.

The nuclear spin steady state is defined as the solution to the following eigenvalue equation:

$$(\mathbb{1} - \mathcal{Y}_n)\mathcal{S}_n = \lambda \mathcal{S}_n, \tag{A4}$$

with $\lambda = 0$. We have kept λ in this equation since we will need to consider nonzero eigenvalues as well in order to obtain the relaxation time. Using the above expansions and equating terms occurring at the same level, we find

$$\begin{aligned} &\left(\mathbb{1} - \mathcal{Y}_n^{(0)}\right)\mathcal{S}_n^{(0)} = 0, \\ &\left(\mathbb{1} - \mathcal{Y}_n^{(0)}\right)\mathcal{S}_n^{(1)} = \left(\mathcal{Y}_n^{(1)} + \lambda_1\right)\mathcal{S}_n^{(0)}, \\ &\left(\mathbb{1} - \mathcal{Y}_n^{(0)}\right)\mathcal{S}_n^{(2)} = \left(\mathcal{Y}_n^{(2)} + \lambda_2\right)\mathcal{S}_n^{(0)} + \left(\mathcal{Y}_n^{(1)} + \lambda_1\right)\mathcal{S}_n^{(1)}. \end{aligned} \tag{A5}$$

In the first of these equations, we have taken the liberty of setting $\lambda_0 = 0$ since the relaxation time will be related to the smallest eigenvalue of $\mathbb{1} - \mathcal{Y}_n$. More specifically, it is apparent from Eq. (A3) that at zeroth order, two of the eigenvalues of $\mathbb{1} - \mathcal{Y}_n^{(0)}$ vanish, so that we have a degenerate perturbation theory. One of these eigenvalues will remain zero at all orders of the perturbative expansion, and the corresponding eigenvector is the effective steady state of the nucleus. The second zero eigenvalue will receive corrections at higher orders. Since these corrections will be proportional to the hyperfine coupling, this will then correspond to the smallest nonzero eigenvalue of $\mathbb{1} - \mathcal{Y}_n$ when the coupling is sufficiently small.

The first equation in (A5) states that the zeroth-order eigenvectors $\mathcal{S}_n^{(0)}$ with vanishing eigenvalues live in the null space of $\mathbb{1} - \mathcal{Y}_n^{(0)}$. It is clear from Eq. (A3) that the null space of $\mathbb{1} - \mathcal{Y}_n^{(0)}$ is spanned by the vectors $v_0 \equiv (1,0,0,0)$ and $v_1 \equiv (0,0,0,1)$. Since the first component of the steady state $\mathcal{S}_{n,ss}$ must be fixed at 1 [see the discussion following Eq. (17)], we may write for the zeroth-order steady state

$$\mathcal{S}_{n,ss}^{(0)} = (1,0,0,\xi), \tag{A6}$$

where ξ is a constant. The fact that the value of ξ is not determined by the zeroth-order equation means that in the absence of hyperfine flip-flops, the nuclear spin steady state is not unique and depends on the initial state. When hyperfine flip-flops are included by taking into account the higher-order equations in (A5), the value of ξ becomes fixed, and the steady state is unique. To see this, we need to solve both the first-order and the second-order equations in (A5).

Consider the first-order equation in (A5). We can dot both sides of this equation by the vectors v_0 and v_1 to obtain

$$v_0\left(\mathcal{Y}_n^{(1)} + \lambda_1\right)\mathcal{S}_n^{(0)} = 0, \quad v_1\left(\mathcal{Y}_n^{(1)} + \lambda_1\right)\mathcal{S}_n^{(0)} = 0. \tag{A7}$$

It is generally the case that the components $\mathcal{Y}_{n,00}^{(1)}$ and $\mathcal{Y}_{n,zz}^{(1)}$ are zero, so that $v_0\mathcal{Y}_n^{(1)}v_0 = v_1\mathcal{Y}_n^{(1)}v_1 = 0$, implying $\lambda_1 = 0$. The reason $\mathcal{Y}_{n,00}^{(1)}$ vanishes is due to the requirement that $\mathcal{Y}_{n,00} = 1$, which must hold for all evolution operators in the 4D SV representation, and which is already satisfied by $\mathcal{Y}_{n,00}^{(0)}$. The

component $\mathcal{Y}^{(1)}_{n,zz}$ vanishes because populations are unaltered in first-order perturbation theory. Since $\lambda_1 = 0$, the relaxation rate will be at least second order in the hyperfine coupling. It is not difficult to directly solve the first-order equation in (A5), with the result

$$\mathcal{S}^{(1)}_n = p_1 + bv_1, \tag{A8}$$

where p_1 is a vector of the form $p_1 = (0, p_{12}, p_{13}, 0)$, which can be obtained explicitly from the formula

$$p_1 = \begin{bmatrix} 1 & 0 & 0 & 0 \\ 0 & X_{xx} & X_{xy} & 0 \\ 0 & X_{yx} & X_{yy} & 0 \\ 0 & 0 & 0 & 1 \end{bmatrix} \mathcal{Y}^{(1)}_n(1,0,0,\xi), \tag{A9}$$

where the 2×2 matrix X is defined as

$$X \equiv \begin{bmatrix} 1 - \mathcal{Y}^{(0)}_{n,xx} & \mathcal{Y}^{(0)}_{n,xy} \\ \mathcal{Y}^{(0)}_{n,yx} & 1 - \mathcal{Y}^{(0)}_{n,yy} \end{bmatrix}^{-1}. \tag{A10}$$

It should be noted that p_1 is a function of the constant ξ. The additional constant b appearing in Eq. (A8) is arbitrary. We do not include a term proportional to v_0 as well because this would violate the constraint that the first component of the 4D SV is fixed to 1 since we have already set the first component of the zeroth-order steady state, $\mathcal{S}^{(0)}_{n,ss}$, to 1.

Dotting both sides of the second-order equation in (A5) by v_1 gives

$$v_1 \mathcal{Y}^{(1)}_n p_1 + v_1 \left(\mathcal{Y}^{(2)}_n + \lambda_2\right) \mathcal{S}^{(0)}_n = 0. \tag{A11}$$

This equation has two solutions:

$$\mathcal{S}^{(0)}_n = (1,0,0,\xi^*), \quad \lambda_2 = 0, \tag{A12}$$

and

$$\mathcal{S}^{(0)}_n = (0,0,0,1), \quad \lambda_2 = \lambda_2^*. \tag{A13}$$

The first solution, Eq. (A12), is the nuclear steady state SV, while the second solution, Eq. (A13), gives the nuclear spin relaxation rate (the rate at which the nuclear spin reaches its steady state):

$$\gamma_n = \lambda_2^*/T_R. \tag{A14}$$

As we anticipated, the nuclear spin steady state is unique in the presence of hyperfine flip-flops. The explicit expressions for ξ^*, λ_2^* depend on the particular control sequence.

APPENDIX B: EFFECTIVE NUCLEAR SPIN EVOLUTION TO SECOND ORDER IN HYPERFINE FLIP-FLOPS FOR SINGLE-PULSE-PER-PERIOD DRIVING

As explained in the previous Appendix, the effective nuclear spin evolution operator in the SV representation can be expanded to second order in the hyperfine flip-flop interaction:

$$\mathcal{Y}_n = \mathcal{Y}^{(0)}_n + \mathcal{Y}^{(1)}_n + \mathcal{Y}^{(2)}_n + \cdots. \tag{B1}$$

In this expansion, we are working in the Markovian limit, and we are retaining the Overhauser part of the interaction to all orders. The explicit form of the zeroth-order evolution in the case of a single pulse per driving period is

$$\mathcal{Y}^{(0)}_n = \begin{bmatrix} 1 & 0 & 0 & 0 \\ 0 & \cos\left(\frac{AT_R}{2}\right)\cos\left(T_R\omega_n\right) - \sin\left(\frac{AT_R}{2}\right)\sin\left(T_R\omega_n\right) S_{e,z} & -\cos\left(\frac{AT_R}{2}\right)\sin\left(T_R\omega_n\right) - \cos\left(T_R\omega_n\right)\sin\left(\frac{AT_R}{2}\right) S_{e,z} & 0 \\ 0 & \cos\left(\frac{AT_R}{2}\right)\sin\left(T_R\omega_n\right) + \cos\left(T_R\omega_n\right)\sin\left(\frac{AT_R}{2}\right) S_{e,z} & \cos\left(\frac{AT_R}{2}\right)\cos\left(T_R\omega_n\right) - \sin\left(\frac{AT_R}{2}\right)\sin\left(T_R\omega_n\right) S_{e,z} & 0 \\ 0 & 0 & 0 & 1 \end{bmatrix}, \tag{B2}$$

and the nonzero components of the first- and second-order contributions are

$$\begin{aligned}
\mathcal{Y}^{(1)}_{n,x0} &= \frac{A \sin\left(\frac{AT_R}{2}\right) \sin\left[\frac{1}{2}T_R(\omega_e - \omega_n)\right]\left\{S_{e,x} \cos\left[\frac{1}{2}T_R(\omega_e + \omega_n)\right] - S_{e,y} \sin\left[\frac{1}{2}T_R(\omega_e + \omega_n)\right]\right\}}{\omega_e - \omega_n}, \\
\mathcal{Y}^{(1)}_{n,xz} &= \frac{A \cos\left(\frac{AT_R}{2}\right) \sin\left[\frac{1}{2}T_R(\omega_e - \omega_n)\right]\left\{S_{e,x} \sin\left[\frac{1}{2}T_R(\omega_e + \omega_n)\right] + S_{e,y} \cos\left[\frac{1}{2}T_R(\omega_e + \omega_n)\right]\right\}}{\omega_e - \omega_n}, \\
\mathcal{Y}^{(1)}_{n,y0} &= \frac{A \sin\left(\frac{AT_R}{2}\right) \sin\left[\frac{1}{2}T_R(\omega_e - \omega_n)\right]\left\{S_{e,x} \sin\left[\frac{1}{2}T_R(\omega_e + \omega_n)\right] + S_{e,y} \cos\left[\frac{1}{2}T_R(\omega_e + \omega_n)\right]\right\}}{\omega_e - \omega_n}, \\
\mathcal{Y}^{(1)}_{n,yz} &= -\frac{A(1 + e^{iAT_R}) e^{-\frac{1}{2}iT_R(A+\omega_e+\omega_n)} \sin\left[\frac{1}{2}T_R(\omega_e - \omega_n)\right]\left[(S_{e,x} + iS_{e,y}) e^{iT_R(\omega_e+\omega_n)} + S_{e,x} - iS_{e,y}\right]}{4(\omega_e - \omega_n)}, \\
\mathcal{Y}^{(1)}_{n,zx} &= -\frac{A\{-S_{e,x} \cos[T_R(\omega_e - \omega_n)] + S_{e,y} \sin[T_R(\omega_e - \omega_n)] + S_{e,x}\}}{2(\omega_e - \omega_n)}, \\
\mathcal{Y}^{(1)}_{n,zy} &= \frac{A(S_{e,x} \sin[T_R(\omega_e - \omega_n)] + S_{e,y}\{\cos[T_R(\omega_e - \omega_n)] - 1\})}{2(\omega_e - \omega_n)},
\end{aligned} \tag{B3}$$

$$
\begin{aligned}
\mathcal{Y}^{(2)}_{n,xx} &= \frac{A^2}{4(\omega_e-\omega_n)^2}\Bigg\{S_{e,z}\sin\left(\frac{AT_R}{2}\right)[T_R(\omega_e-\omega_n)\cos(\omega_n T_R)-\sin(\omega_e T_R)+\sin(\omega_n T_R)]\\
&\quad+\cos\left(\frac{AT_R}{2}\right)[T_R(\omega_e-\omega_n)\sin(\omega_n T_R)+\cos(\omega_e T_R)-\cos(\omega_n T_R)]\Bigg\},\\
\mathcal{Y}^{(2)}_{n,xy} &= \frac{A^2}{4(\omega_e-\omega_n)^2}\Bigg\{S_{e,z}\sin\left(\frac{AT_R}{2}\right)[T_R(\omega_n-\omega_e)\sin(\omega_n T_R)-\cos(\omega_e T_R)+\cos(\omega_n T_R)]\\
&\quad+\cos\left(\frac{AT_R}{2}\right)(T_R(\omega_e-\omega_n)\cos(\omega_n T_R)-\sin(\omega_e T_R)+\sin(\omega_n T_R)]\Bigg\},\\
\mathcal{Y}^{(2)}_{n,yx} &= \frac{A^2}{4(\omega_e-\omega_n)^2}\Bigg\{S_{e,z}\sin\left(\frac{AT_R}{2}\right)[T_R(\omega_e-\omega_n)\sin(\omega_n T_R)+\cos(\omega_e T_R)-\cos(\omega_n T_R)]\\
&\quad+\cos\left(\frac{AT_R}{2}\right)[T_R(\omega_n-\omega_e)\cos(\omega_n T_R)+\sin(\omega_e T_R)-\sin(\omega_n T_R)]\Bigg\},\\
\mathcal{Y}^{(2)}_{n,yy} &= \frac{A^2}{4(\omega_e-\omega_n)^2}\Bigg\{S_{e,z}\sin\left(\frac{AT_R}{2}\right)[T_R(\omega_e-\omega_n)\cos(\omega_n T_R)-\sin(\omega_e T_R)+\sin(\omega_n T_R)]\\
&\quad+\cos\left(\frac{AT_R}{2}\right)[T_R(\omega_e-\omega_n)\sin(\omega_n T_R)+\cos(\omega_e T_R)-\cos(\omega_n T_R)]\Bigg\},\\
\mathcal{Y}^{(2)}_{n,z0} &= \frac{A^2 S_{e,z}\sin^2\left[\frac{1}{2}T_R(\omega_e-\omega_n)\right]}{(\omega_e-\omega_n)^2},\quad \mathcal{Y}^{(2)}_{n,zz}=\frac{A^2\{\cos[T_R(\omega_e-\omega_n)]-1\}}{2(\omega_e-\omega_n)^2}.
\end{aligned}
\tag{B4}
$$

APPENDIX C: NUCLEAR SPIN STEADY STATE AND RELAXATION RATE FOR SINGLE-PULSE-PER-PERIOD DRIVING

In the case of driving with a single pulse per period as considered in Sec. V F and which is relevant for the mode-locking experiments analyzed in detail in Sec. VI, the explicit forms of the nuclear spin steady and relaxation rate for arbitrary nuclear Zeeman energy ω_n are

$$
\mathcal{S}_n^{(\infty)} = (1,0,0,\xi^*),\quad \gamma_n = \lambda_2^*/T_R,
\tag{C1}
$$

with

$$
\xi^* = S_{n,z}^{(\infty)} = \frac{C}{D},\quad \lambda_2^* = \frac{A^2}{4(\omega_e-\omega_n)^2}(2-F/G),
\tag{C2}
$$

where

$$
C = -2e^{iT_R(A+\omega_n)}\left\{2\left(S_{e,z}^2+S_e^2\right)\sin\left(\frac{AT_R}{2}\right)\sin(\omega_n T_R)+S_{e,z}\left[-\left(S_e^2-1\right)\cos(AT_R)-4\cos\left(\frac{AT_R}{2}\right)\cos(\omega_n T_R)+S_e^2+3\right]\right\},
\tag{C3}
$$

$$
\begin{aligned}
D &= \left[(S_{e,z}-2)S_{e,z}-S_e^2+2\right]e^{\frac{1}{2}iT_R(A+4\omega_n)}+2\left(-2S_{e,z}^2+S_e^2-3\right)e^{iT_R(A+\omega_n)}+\left[S_{e,z}(S_{e,z}+2)-S_e^2+2\right]e^{\frac{1}{2}iT_R(3A+4\omega_n)}\\
&\quad+e^{\frac{3}{2}iAT_R}\left[(S_{e,z}-2)S_{e,z}-S_e^2+2\right]+e^{\frac{1}{2}iAT_R}\left[S_{e,z}(S_{e,z}+2)-S_e^2+2\right]+\left(S_e^2-1\right)e^{iT_R(2A+\omega_n)}+\left(S_e^2-1\right)e^{i\omega_n T_R},
\end{aligned}
\tag{C4}
$$

$$
\begin{aligned}
F &= 2(\xi-1)S_{e,\perp}^2\cos\left[\frac{1}{2}T_R(A-2\omega_n)\right]+2(\xi+1)S_{e,\perp}^2\cos\left[\frac{1}{2}T_R(A+2\omega_n)\right]\\
&\quad+\left[-(\xi-1)S_{e,\perp}^2-2S_{e,z}+2\right]\cos\left[\frac{1}{2}T_R(A+2\omega_e-4\omega_n)\right]+\left[(\xi-S_{e,z})S_{e,\perp}^2+S_{e,z}^2-1\right]\cos[T_R(A+\omega_e-\omega_n)]\\
&\quad+\left[(\xi-S_{e,z})S_{e,\perp}^2+S_{e,z}^2-1\right]\cos[T_R(A-\omega_e+\omega_n)]-\left[(\xi+1)S_{e,\perp}^2-2(S_{e,z}+1)\right]\cos\left[\frac{1}{2}T_R(A-2\omega_e+4\omega_n)\right]
\end{aligned}
$$

$$-2\cos\left(\frac{AT_R}{2}\right)\cos(\omega_e T_R)\left[\xi S_{e,\perp}^2-2\right]-2S_{e,\perp}^2[\cos(AT_R)(\xi-S_{e,z})+S_{e,z}+\xi]$$

$$+2\cos[T_R(\omega_e-\omega_n)]\left[\xi S_{e,\perp}^2+S_{e,z}\left(S_{e,\perp}^2-S_{e,z}\right)-3\right]+2\sin\left(\frac{AT_R}{2}\right)\sin(\omega_e T_R)\left(S_{e,\perp}^2-2S_{e,z}\right), \tag{C5}$$

$$G=-4S_{e,z}\sin\left(\frac{AT_R}{2}\right)\sin(\omega_n T_R)+\left(S_{e,z}^2-1\right)\cos(AT_R)-S_{e,z}^2+4\cos\left(\frac{AT_R}{2}\right)\cos(\omega_n T_R)-3. \tag{C6}$$

In the above expressions, we have compressed the notation for the electron steady state $S_{e,i}^{(\infty)}\to S_{e,i}$ for the sake of brevity, and we have defined $S_e^2\equiv S_{e,x}^2+S_{e,y}^2+S_{e,z}^2$.

APPENDIX D: DERIVATION OF FLIP-RATE EXPRESSION

At leading order in the hyperfine coupling, the nuclei are essentially independent of each other, and we may estimate the flip rates by using the solution we have obtained for the single-nucleus problem. For a single nucleus, we may write

$$\frac{dP_\uparrow}{dt}=-\mathrm{w}_- P_\uparrow+\mathrm{w}_+ P_\downarrow, \tag{D1}$$

where $P_\uparrow$ is the probability that the nucleus is aligned with the magnetic field and $P_\downarrow=1-P_\uparrow$ is the probability that it lies antiparallel to the magnetic field. In terms of the nuclear SV component along the magnetic field direction, $S_{n,z}$, these probabilities are given by

$$P_\uparrow=\tfrac{1}{2}(1+S_{n,z}),\quad P_\downarrow=\tfrac{1}{2}(1-S_{n,z}). \tag{D2}$$

Therefore, we have

$$\frac{d}{dt}S_{n,z}=-(\mathrm{w}_++\mathrm{w}_-)S_{n,z}+\mathrm{w}_+-\mathrm{w}_-. \tag{D3}$$

The solution to this equation is easily obtained:

$$S_{n,z}(t)=\left[S_{n,z}(0)-\frac{\mathrm{w}_+-\mathrm{w}_-}{\mathrm{w}_++\mathrm{w}_-}\right]e^{-(\mathrm{w}_++\mathrm{w}_-)t}+\frac{\mathrm{w}_+-\mathrm{w}_-}{\mathrm{w}_++\mathrm{w}_-}. \tag{D4}$$

We may then compute the flip rates $\mathrm{w}_\pm$ by comparing this with our coarse-grained solution from Eq. (25):

$$\mathcal{S}_n(t)=e^{(\mathcal{Y}_n-1)t/T_R}\mathcal{S}_n(0). \tag{D5}$$

To facilitate the comparison, we expand the initial state as a linear combination of the eigenvectors of $1-\mathcal{Y}_n$:

$$\mathcal{S}_n(0)=\mathcal{S}_n^{(\infty)}+\sum_{i=1}^{3}c_i\mathcal{V}_i. \tag{D6}$$

Here we have set the coefficient of the steady state $\mathcal{S}_n^{(\infty)}$ to 1 since the first component of $\mathcal{S}_n(0)$ must be 1, and the first component of $\mathcal{S}_n^{(\infty)}$ is already 1. (Consequently, it must be the case that the first components of each of the $\mathcal{V}_i$ are all zero.) Plugging Eq. (D6) into Eq. (D5), we find

$$\mathcal{S}_n(t)=\mathcal{S}_n^{(\infty)}+\sum_{i=1}^{3}c_i e^{-\mu_i t/T_R}\mathcal{V}_i, \tag{D7}$$

where the μ_i are the eigenvalues of $1-\mathcal{Y}_n$ corresponding to the $\mathcal{V}_i$.

At this point, we use the fact that the null space of $1-\mathcal{Y}_n^{(0)}$ is twofold degenerate and spanned by the vectors $v_0=(1,0,0,0)$ and $v_1=(0,0,0,1)$, as discussed in Appendix A. Two of the four eigenvectors will therefore have a vanishing eigenvalue at zeroth order in perturbation theory. One of these eigenvectors is the steady state $\mathcal{S}_n^{(\infty)}$, and we choose the other to be $\mathcal{V}_3$. This immediately implies that the steady state has the form $\mathcal{S}_n^{(\infty)}=(1,0,0,\xi^*)$, while $\mathcal{V}_3=(0,0,0,1)$ at zeroth order since the first component of $\mathcal{S}_n^{(\infty)}$ is 1, while that of $\mathcal{V}_3$ has to be zero. Since the null space is orthogonal to the row space spanned by $\mathcal{V}_1$ and $\mathcal{V}_2$, these vectors must be orthogonal to v_0 and v_1 at zeroth order and therefore do not have z components at zeroth order. Taking the z component of Eq. (D7), we find that the zeroth-order nuclear spin z component is given by

$$\mathcal{S}_{n,z}(t)=S_{n,z}^{(\infty)}+c_3 e^{-\mu_3 t/T_R}. \tag{D8}$$

Identifying μ_3/T_R as the nuclear spin relaxation rate γ_n, and rewriting c_3 in terms of the initial value $S_{n,z}(0)$, we have

$$S_{n,z}(t)=\left[S_{n,z}(0)-S_{n,z}^{(\infty)}\right]e^{-\gamma_n t}+S_{n,z}^{(\infty)}. \tag{D9}$$

Comparing this equation with Eq. (D4) gives

$$\mathrm{w}_\pm=\gamma_n\left(1\pm S_{n,z}^{(\infty)}\right)/2, \tag{D10}$$

which is quoted in Eq. (31).

APPENDIX E: CONTINUUM OF RATE EQUATION

Starting from the recursion formula for the nuclear spin polarization distribution,

$$P(m)=\frac{N-m+2}{N+m}\frac{w_+(m-2)}{w_-(m)}P(m-2), \tag{E1}$$

we can take the continuum limit by rewriting this as

$$w_-(m+2)P(m+2)-w_-(m)P(m)=\frac{N-m}{N+m+2}w_+(m)P(m)-w_-(m)P(m). \tag{E2}$$

Defining the function $\Phi(m)\equiv w_-(m)P(m)$, we can interpret the left-hand side as the derivative of Φ in the continuum limit:

$$\Phi'(m)=\frac{1}{2}\left[\frac{N-m}{N+m+2}\frac{w_+(m)}{w_-(m)}-1\right]\Phi(m). \tag{E3}$$

This equation is easily integrated, with the result

$$\Phi(m) = C \exp\left\{\frac{1}{2}\int_{-N}^{m} dm' \left[\frac{N-m'}{N+m'+2}\frac{w_+(m')}{w_-(m')} - 1\right]\right\}. \tag{E4}$$

The constant C is determined by the normalization of $P(m)$:

$$C = \left[\sum_m \frac{\exp\left\{\frac{1}{2}\int_{-N}^{m} dm' \left[\frac{N-m'}{N+m'+2}\frac{w_+(m')}{w_-(m')} - 1\right]\right\}}{w_-(m)}\right]^{-1}. \tag{E5}$$

In the special case where the flip rates are equal, $w_+(m) = w_-(m)$, the polarization distribution reduces to

$$P(m) = \frac{2^{-1-m-N} C e^{-m-N} (2+m+N)^{1+N}}{w_-(m)}. \tag{E6}$$

It is clear from this expression that the zeros of $w_-(m)$ give rise to peaks in $P(m)$. For the original mode-locking experiment, $w_-(m) \sim \sin^2[(\omega_e + Am/2)T_R/2]$, while in the case of spin echo, $w_-(m) \sim \sin^2[(\omega_e + Am/2)T_R/4]$, immediately implying that $P(m)$ will exhibit a comblike structure in both cases.

[1] K. Ono and S. Tarucha, Phys. Rev. Lett. **92**, 256803 (2004).
[2] A. S. Bracker, E. A. Stinaff, D. Gammon, M. E. Ware, J. G. Tischler, A. Shabaev, A. L. Efros, D. Park, D. Gershoni, V. L. Korenev *et al.*, Phys. Rev. Lett. **94**, 047402 (2005).
[3] F. H. L. Koppens, C. Buizert, K. J. Tielrooij, I. T. Vink, K. C. Nowack, T. M. L. P. Kouwenhoven, and L. M. K. Vandersypen, Nature (London) **442**, 766 (2006).
[4] A. Greilich, A. Shabaev, D. R. Yakovlev, A. L. Efros, I. A. Yugova, D. Reuter, A. D. Wieck, and M. Bayer, Science **317**, 1896 (2007).
[5] C. Latta, A. Högele, Y. Zhao, A. N. Vamivakas, P. Maletinsky, M. Kroner, J. Dreiser, I. Carusotto, A. Badolato, D. Schuh *et al.*, Nat. Phys. **5**, 758 (2009).
[6] X. Xu, W. Yao, B. Sun, D. G. Steel, A. S. Bracker, D. Gammon, and L. J. Sham, Nature (London) **459**, 1105 (2009).
[7] I. T. Vink, K. C. Nowack, F. Koppens, J. Danon, Y. V. Nazarov, and L. M. K. Vandersypen, Nat. Phys. **5**, 764 (2009).
[8] C. Kloeffel, P. A. Dalgarno, B. Urbaszek, B. D. Gerardot, D. Brunner, P. M. Petroff, D. Loss, and R. J. Warburton, Phys. Rev. Lett. **106**, 046802 (2011).
[9] I. A. Merkulov, A. L. Efros, and M. Rosen, Phys. Rev. B **65**, 205309 (2002).
[10] W. A. Coish and D. Loss, Phys. Rev. B **70**, 195340 (2004).
[11] C. Deng and X. Hu, Phys. Rev. B **73**, 241303(R) (2006).
[12] W. Yao, R.-B. Liu, and L. J. Sham, Phys. Rev. B **74**, 195301 (2006).
[13] Ł. Cywiński, W. M. Witzel, and S. Das Sarma, Phys. Rev. B **79**, 245314 (2009).
[14] W. A. Coish, J. Fischer, and D. Loss, Phys. Rev. B **81**, 165315 (2010).
[15] B. Erbe and J. Schliemann, Phys. Rev. Lett. **105**, 177602 (2010).
[16] A. Faribault and D. Schuricht, Phys. Rev. Lett. **110**, 040405 (2013).
[17] S. Foletti, H. Bluhm, D. Mahalu, V. Umansky, and A. Yacoby, Nat. Phys. **5**, 903 (2009).
[18] J. M. Taylor, A. Imamoglu, and M. D. Lukin, Phys. Rev. Lett. **91**, 246802 (2003).
[19] M. S. Rudner and L. S. Levitov, Phys. Rev. Lett. **99**, 036602 (2007).
[20] E. Barnes, Ł. Cywiński, and S. Das Sarma, Phys. Rev. Lett. **109**, 140403 (2012).
[21] J. Baugh, Y. Kitamura, K. Ono, and S. Tarucha, Phys. Rev. Lett. **99**, 096804 (2007).
[22] H. Bluhm, S. Foletti, D. Mahalu, V. Umansky, and A. Yacoby, Phys. Rev. Lett. **105**, 216803 (2010).
[23] G. Petersen, E. A. Hoffmann, D. Schuh, W. Wegscheider, G. Giedke, and S. Ludwig, Phys. Rev. Lett. **110**, 177602 (2013).
[24] B. Urbaszek, X. Marie, T. Amand, O. Krebs, P. Voisin, P. Maletinsky, A. Högele, and A. Imamoglu, Rev. Mod. Phys. **85**, 79 (2013).
[25] E. A. Chekhovich, M. N. Makhonin, A. I. Tartakovskii, A. Yacoby, B. H., K. C. Nowack, and L. M. K. Vandersypen, Nat. Mater. **12**, 494 (2013).
[26] A. Högele, M. Kroner, C. Latta, M. Claassen, I. Carusotto, C. Bulutay, and A. Imamoglu, Phys. Rev. Lett. **108**, 197403 (2012).
[27] J. Nilsson, L. Bouet, A. J. Bennett, T. Amand, R. M. Stevenson, I. Farrer, D. A. Ritchie, S. Kunz, X. Marie, A. J. Shields *et al.*, Phys. Rev. B **88**, 085306 (2013).
[28] C. Deng and X. Hu, Phys. Rev. B **71**, 033307 (2005).
[29] M. Gullans, J. J. Krich, J. M. Taylor, H. Bluhm, B. I. Halperin, C. M. Marcus, M. Stopa, A. Yacoby, and M. D. Lukin, Phys. Rev. Lett. **104**, 226807 (2010).
[30] I. Neder, M. S. Rudner, and B. I. Halperin, Phys. Rev. B **89**, 085403 (2014).
[31] M. S. Rudner, L. M. K. Vandersypen, V. Vuletić, and L. S. Levitov, Phys. Rev. Lett. **107**, 206806 (2011).
[32] M. Gullans, J. J. Krich, J. M. Taylor, B. I. Halperin, and M. D. Lukin, Phys. Rev. B **88**, 035309 (2013).
[33] M. J. A. Schuetz, E. M. Kessler, L. M. K. Vandersypen, J. I. Cirac, and G. Giedke, Phys. Rev. Lett. **111**, 246802 (2013).
[34] A. Brataas and E. I. Rashba, Phys. Rev. Lett. **109**, 236803 (2012).
[35] W. Yang and L. J. Sham, Phys. Rev. B **85**, 235319 (2012).
[36] W. Yang and L. J. Sham, Phys. Rev. B **88**, 235304 (2013).
[37] X.-F. Shi, Phys. Rev. B **87**, 195318 (2013).
[38] M. Issler, E. M. Kessler, G. Giedke, S. Yelin, I. Cirac, M. D. Lukin, and A. Imamoglu, Phys. Rev. Lett. **105**, 267202 (2010).
[39] E. Barnes and S. E. Economou, Phys. Rev. Lett. **107**, 047601 (2011).
[40] S. G. Carter, A. Shabaev, S. E. Economou, T. A. Kennedy, A. S. Bracker, and T. L. Reinecke, Phys. Rev. Lett. **102**, 167403 (2009).
[41] S. G. Carter, S. E. Economou, A. Shabaev, and A. S. Bracker, Phys. Rev. B **83**, 115325 (2011).
[42] An alternative approach to the mode-locking experiment was recently given in Ref. [43].

[43] M. M. Glazov, I. A. Yugova, and Al. L. Efros, Phys. Rev. B **85**, 041303(R) (2012).
[44] S. G. Carter, S. E. Economou, A. Greilich, E. Barnes, T. Sweeney, A. S. Bracker, and D. Gammon, Phys. Rev. B **89**, 075316 (2014).
[45] J. Javanainen, Europhys. Lett. **17**, 407 (1992).
[46] S. E. Economou, R.-B. Liu, L. J. Sham, and D. G. Steel, Phys. Rev. B **71**, 195327 (2005).
[47] M. V. G. Dutt, J. Cheng, B. Li, X. Xu, X. Li, P. R. Berman, D. G. Steel, A. S. Bracker, D. Gammon, S. E. Economou *et al*., Phys. Rev. Lett. **94**, 227403 (2005).
[48] A. W. Overhauser, Phys. Rev. **92**, 411 (1953).
[49] T. R. Carver and C. P. Slichter, Phys. Rev. **102**, 975 (1956).
[50] A similar model was recently considered in Ref. [51].
[51] N. Wu, W. Ding, A. Shi, and W. Zhang, arXiv:1303.0590.
[52] M. A. Nielsen and I. L. Chuang, *Quantum Computation and Quantum Information* (Cambridge University Press, Cambridge, UK, 2000).
[53] E. Barnes, Ł. Cywiński, and S. Das Sarma, Phys. Rev. B **84**, 155315 (2011).
[54] S. E. Economou, L. J. Sham, Y. Wu, and D. G. Steel, Phys. Rev. B **74**, 205415 (2006).